ISSN 2472-1972

Amhr2-Cre–Mediated Global *Tspo* Knockout

Jinjiang Fan,[1,2] Enrico Campioli,[1,2] Chantal Sottas,[3] Barry Zirkin,[4] and Vassilios Papadopoulos[1,2,3]

[1]The Research Institute of the McGill University Health Centre; [2]Department of Medicine, McGill University, Montreal, Quebec H4A 3J1, Canada; [3]Department of Pharmacology and Pharmaceutical Sciences, School of Pharmacy, University of Southern California, Los Angeles, California 90089, US; and [4]Department of Biochemistry and Molecular Biology, Johns Hopkins Bloomberg School of Public Health, Baltimore, Maryland 21205, US

ORCiD numbers: 0000-0002-1183-8568 (V. Papadopoulos).

Although the role of translocator protein (TSPO) in cholesterol transport in steroid-synthesizing cells has been studied extensively, recent studies of TSPO genetic depletion have questioned its role. *Amhr2*-Cre mice have been used to generate Leydig cell-specific *Tspo* conditional knockout (cKO) mice. Using the same Cre line, we were unable to generate *Tspo* cKO mice possibly because of genetic linkage between *Tspo* and *Amhr2* and coexpression of *Amhr2*-Cre and *Tspo* in early embryonic development. We found that *Amhr2*-Cre is expressed during preimplantation stages, resulting in global heterozygous mice (gHE; *Amhr2*-Cre$^{+/-}$,*Tspo*$^{-/+}$). Two gHE mice were crossed, generating *Amhr2*-Cre–mediated *Tspo* global knockout (gKO; *Tspo*$^{-/-}$) mice. We found that 33.3% of blastocysts at E3.5 to E4.5 showed normal morphology, whereas 66.7% showed delayed development, which correlates with the expected Mendelian proportions of *Tspo*$^{+/+}$ (25%), *Tspo*$^{-/-}$ (25%), and *Tspo*$^{+/-}$ (50%) genotypes from crossing 2 *Tspo*$^{-/+}$ mice. Adult *Tspo* gKO mice exhibited disturbances in neutral lipid homeostasis and reduced intratesticular and circulating testosterone levels, but no change in circulating basal corticosterone levels. RNA-sequencing data from mouse adrenal glands and lungs revealed transcriptome changes in response to the loss of TSPO, including changes in several cholesterol-binding and transfer proteins. This study demonstrates that *Amhr2*-Cre can be used to produce *Tspo* gKO mice instead of cKO, and can serve as a new global "Cre deleter." Moreover, our results show that *Tspo* deletion causes delayed preimplantation embryonic development, alters neutral lipid storage and steroidogenesis, and leads to transcriptome changes that may reflect compensatory mechanisms in response to the loss of function of TSPO.

Key Words: translocator protein, genetic linkage, global knockout, steroid, testosterone, cholesteryl esters, autophagy, compensatory genetic network.

Translocator protein (TSPO) is an outer mitochondrial membrane protein with multiple biological functions, including direct or indirect roles in mitochondrial cholesterol transport and steroid hormone biosynthesis, porphyrin transport and heme synthesis, apoptosis, cell proliferation, and anion transport [1]. TSPO is expressed at high levels in steroid-synthesizing tissues and binds with high affinity to cholesterol and numerous other compounds [2]. The role of TSPO in steroid biosynthesis has been extensively investigated in studies of the function of TSPO in multiple protein complexes involved in mitochondrial cholesterol transport, as well as animal models of disease [3-7]. However, recently published studies of the genetic

Abbreviations: ACTH, adrenocorticotropic hormone; *Amhr2*-Cre, anti-Müllerian hormone receptor type 2-Cre; cKO, conditional knockout; gHE, global heterozygous; gHO, global homozygous; gKO, global knockout; KO, knockout; TSPO, translocator protein; WT, wild-type.

Received 29 July 2019
Accepted 9 January 2020
First Published Online 12 January 2020
Corrected and Typeset 19 February 2020.

depletion of TSPO have produced conflicting findings regarding the role of TSPO in steroid biosynthesis, heme synthesis, and the function of the TSPO diagnostic ligand PK 11195 in steroid production [8-11].

To reproduce previous results obtained with Leydig cell-targeted *Tspo* conditional knockout (cKO) mice, showing a lack of effect on androgen production [8], we started with the same *Amhr2*-Cre (anti-Müllerian hormone receptor type 2-Cre) mice, but did not succeed in generating mice with the loss of the TSPO protein [12]. However, using a different Cre line (*Nr5a1*-Cre or *Sf1*-Cre), we generated steroidogenic cell-targeted *Tspo* cKO mice that showed a congenital adrenal hyperplasia-like phenotype with lipid accumulation accompanied by the lack of ability to produce corticosterone in response to adrenocorticotropic hormone (ACTH) [12]. This phenotype is similar to that of *Star* KO mice, which show an accumulation of lipid droplets (LDs) in the adrenal glands [13]. Recently, we used zinc finger nuclease technology to perform *Tspo*-targeted genome editing in the rat and generated 2 lines, a null mutant lacking TSPO expression and a line expressing a truncated TSPO protein lacking the fifth transmembrane domain, containing the cholesterol recognition amino acid consensus motif [14, 15]. Both *Tspo* mutations in rat models led to accumulation of esterified cholesterol in all steroidogenic cells examined and attenuated response to ACTH in terms of corticosteroid formation. Basal testosterone production was also reduced in *Tspo* homozygous (HO) mutant rats. In humans, the presence of the rs6971 polymorphism in the *TSPO* gene, a nonconservative amino acid substitution Ala147Thr, in the fifth transmembrane domain, results in altered binding affinity of TSPO for specific ligands and cholesterol, as well as reduction in ACTH-induced corticosteroid production [14, 16]. Both studies showed experimental evidence of the role of TSPO in steroidogenesis.

One unsolved question about the *Amhr2*-Cre–mediated *Tspo* cKO is that the data presented from the previous 2 reports are in contradiction with each other [8, 12]. One possible explanation is based on the small number of mice (*Amhr2*-Cre$^{+/-}$, *Tspo*$^{fl/fl}$) with a wild-type (WT) phenotype but no conditional target gene deletion [12] because of a suggested strong genetic linkage between *Amhr2* and *Tspo* genes [17]. However, the authors who first reported the *Amhr2*-Cre–mediated cKO type of *Tspo* [8] and later suggested the genetic linkage [17] failed to explain why there was no strong genetic linkage in their own animal study using the same Cre line, in which the same mice (*Amhr2*-Cre$^{+/-}$, *Tspo*$^{fl/fl}$) had a WT phenotype, including no dramatic differences in steroid production [8]. We speculate the presence of, at least, some mixed genotypes in the mouse population in the original study [8].

In the present report, we elucidate in detail the discrepancy between the Morohaku et al paper [8] in which the *Amhr2*-Cre/LoxP system was used to generate a Leydig cell-specific *Tspo* cKO mouse, and our own work to replicate these findings [12]. We also present a new and fully characterized *Amhr2*-Cre–mediated *Tspo* deletion. At the same time we took the opportunity to address criticisms aimed at our work [12] by Selvaraj et al [17], using strong experimental evidence that the early expression of *Amhr2* may hinder the generation of cKO mice. Indeed, the early expression of *Amhr2* at 2- to 4-cell stages of preimplantation embryos was proven to be functional in Rosa-mT/mG$^{+/-}$ mice, leading to the production of *Tspo* global KO genotypes (*Amhr2*-Cre$^{+/-}$, *Tspo*$^{+/-}$ and *Amhr2*-Cre$^{+/-}$, *Tspo*$^{-/-}$). Furthermore, we found that there were adverse effects of the *Tspo* deletion on preimplantation development; abnormal neutral lipid storage, testosterone formation, and transcriptional changes.

1. Material and Methods

A. Generation of Anti-Müllerian Hormone Type 2 Receptor-Cre–Mediated Global Tspo *Knockout Mice*

We previously generated *Amhr2*-Cre–mediated gonadal-specific *Tspo* cKO mice in which the resulting conditional homozygous (cHO) mice appeared to possess WT phenotypes and to represent an unexpectedly small proportion (4.4%) of the total number of pups examined

[8, 12]. This is the same Cre-LoxP KO system used with 2 different genotyping/breeding regimens; we demonstrate in this report that the previously assumed cKO is a global knockout (gKO). To avoid confusion on the nomenclature of the mice used and generated, their corresponding genotypes are presented in Table 1. Considering the genetic linkage between *Amhr2* and *Tspo,* as well as the early expression of *Amhr2*-Cre at 2- to 4-cell stages, we selected expected conditional heterozygous (cHE) mice with a WT-like genotype (*Amhr2*-Cre$^{+/-}$, *Tspo*$^{-/+}$) to screen via specific polymerase chain reaction (PCR) for the deleted exon 2/exon3 flanked by the 2 LoxP sites using the primer sets shown in Table 2: gKO-R/gKO-F to give 3818 base pairs (bp) for WT mice, 4092 bp for *Tspo*-floxed mice, 196 bp for global heterozygous mice (gHE) mice; and exon2-RR/exon2-FF to give 300 bp for WT (*Tspo*$^{+/+}$) and global KO (gKO; *Tspo*$^{+/-}$ and *Tspo*$^{-/-}$) mice. The generated global *Tspo* heterozygous KO (gHE: *Amhr2*-Cre$^{+/-}$, *Tspo*$^{-/+}$) mice were confirmed by sequencing the amplicons. To produce global *Tspo* HO KO (global homozygous [gHO]: *Tspo*$^{-/-}$) mice, 2 gHE mice were crossed to obtain pups for further investigation. Genotyping the generated pups showed the expected 25% gHO, 25% WT, and 50% gHE ratios. Adult mice were weighed and tissues collected, weighed, and processed for further analysis. This study was carried out in accordance with the recommendations of the Canadian Council on Animal Care. The protocol was approved by the McGill University Animal Care Committee and the University of Southern California Institutional Animal Care and Use Committee.

Rosa-mT/mG$^{+/-}$ mice were purchased from the Jackson Laboratory (catalog No. 007576). Genotyping was performed using the following primer sets: WT-F(common): 5'-CTTCCCTCGTGATCTGCAAC-3' with MUT-R: 5'-CAATAGGGGGCGTACTTGG-3' (325 bp for positive mT/mG), and with WT-R: 5'-CCTCCCATTTTCCTTATTTGC-3' (200 bp for negative mT/mG). Mouse blastocysts from *Amhr2*-Cre$^{+/-}$; Rosa-mT/mG$^{+/-}$ mice were harvested between E3.5 and cultured overnight to E4.5. The day of vaginal plug detection was considered to be E0.5.

Table 1. List of mice used and generated, and their corresponding genotypes

Abbreviation	Full Name	Genotype
Amhr2-Cre	*Amhr2*-Cre–positive mouse (WT)	*Amhr2*-Cre$^{+/-}$, *Tspo*$^{+/+}$
WT	C57BL/6J mouse (WT)	*Amhr2*-Cre$^{-/-}$, *Tspo*$^{+/+}$
Tspo cKO	*Amhr2*-Cre–mediated *Tspo* conditional KO	*Amhr2*-Cre$^{+/-}$, *Tspo*$^{+/fl}$ and *Amhr2*-Cre$^{+/-}$, *Tspo*$^{fl/fl}$
WT (mT/mG)	*Amhr2*-Cre$^{-/-}$ reporter mouse	*Amhr2-Cre*$^{-/-}$; *Rosa-mmT/G*$^{+/-}$
WT *(Amhr2-Cre/mG)*	*Amhr2*-Cre$^{+/-}$ reporter mouse	*Amhr2-Cre*$^{+/-}$; *Rosa-mG*$^{+/-}$
Tspo gKO	*Amhr2*-Cre–mediated *Tspo* global KO	*Amhr2*-Cre$^{+/-}$, *Tspo*$^{+/-}$ and *Amhr2*-Cre$^{+/-}$, *Tspo*$^{-/-}$
WT (Fl/Fl)	WT mouse with homozygous floxed *Tspo* alleles	*Amhr2*-Cre$^{-/-}$, *Tspo*$^{fl/fl}$
WT (Fl/+)	WT mouse with heterozygous floxed *Tspo* alleles	*Amhr2*-Cre$^{-/-}$, *Tspo*$^{+/fl}$
cHE	*Amhr2*-Cre–positive, heterozygous floxed *Tspo* alleles	*Amhr2*-Cre$^{+/-}$, *Tspo*$^{+/fl\alpha}$ or *Amhr2*-Cre$^{+/-}$, *Tspo*$^{+/fl}$
"WT-like" gHE	*Amhr2*-Cre–positive, genotyped nonfloxed *Tspo* alleles	*Amhr2*-Cre$^{+/-}$, *Tspo*$^{-/+}$
cHO	*Amhr2*-Cre–positive, homozygous floxed *Tspo* alleles	*Amhr2*-Cre$^{+/-}$, *Tspo*$^{fl\alpha/fl}$ and *Amhr2*-Cre$^{+/-}$, *Tspo*$^{-/fl\alpha}$
"cHO-like" gHE	*Amhr2*-Cre–positive, genotyped homozygous floxed *Tspo* alleles	*Amhr2*-Cre$^{+/-}$, *Tspo*$^{-/fl\alpha}$
Missing gHO	*Amhr2*-Cre–positive, genotyped cKO (nonreaction)	*Amhr2*-Cre$^{+/-}$, *Tspo*$^{-/-}$
gHO	Deleted both *Tspo* alleles	*Tspo*$^{-/-}$
gHE	Deleted one *Tspo* allele	*Tspo*$^{+/-}$
Cre reporter	Rosa-mT/mG	*Tspo*$^{+/+}$, *mT/mG*$^{+/-}$

Abbreviations: *Amhr2*-Cre, anti-Müllerian hormone type 2 receptor-Cre; cHE, conditional heterozygous; cKO, conditional knockout; Fl, floxed; gHE, global heterozygous; gHO, global homozygous; KO, knockout; WT, wild-type.
[a]The floxed allele seems to be defective while it passes through the embryonic stages without target gene deletion.

Table 2. Oligonucleotides used in this study

Primers	Sequence	Purpose
gKO-R	ACCCAGAGTTTGCCAATTGC	Global KO
gKO-F	ATCTCATTACGGGTGGTTGC	Global KO
Exon2-RR	TTGTAGAACTGCCCTCACCCCTACC	WT
Exon2-FF	ATTCCAGGGGCAACAGAGCACAGC	WT
WT-F(c)	CTTCCCTCGTGATCTGCAAC	mT/mG
MUT-R	CAATAGGGGGCGTACTTGG	mT/mG
WT-R	CCTCCCATTTTCCTTATTTGC	mT/mG
Abcb6-F	GTTAGCAATGGTGTCGTTGAAG	Real-time PCR
Abcb6-R	CTGGCTGCATCCGAATAGAT	Real-time PCR
Apoo-F	TTTGGGTGCTGCATAGACTC	Real-time PCR
Apoo-R	TGCCAGCGACATGTTCAA	Real-time PCR
Hprt-R	GCGTCGTGATTAGCGATGATGAAC	Reference gene
Hprt-F	GAGCAAGTCTTTCAGTCCTGTCCA	Real-time PCR
Nr4a2-F	CTGCTGGATATGTTGGGTATCA	Real-time PCR
Nr4a2-R	TCGATTCCAATCCGGCAAT	Real-time PCR
Trim5-F	TCTGACTGAACATTCTCCACATC	Real-time PCR
Trim5-R	GGCTGATGGCAGATAAGAAAGA	Real-time PCR
Trp53inp2-F	GGGTAACAAACCAGCTCTCATC	Real-time PCR
Trp53inp2-R	TGGCTCATCATCGACCTACA	Real-time PCR
Ucp1-F	TGGTCCCTAGGACACCTTTAT	Real-time PCR
Ucp1-R	CCTGGCAGATATCATCACCTTC	Real-time PCR
Ucp2-F	AAGCGGACCTTTACCACATC	Real-time PCR
Ucp2-R	GCCTCTACGACTCTGTCAAAC	Real-time PCR

Abbreviations: cHE, conditional heterozygous; cKO, conditional knockout; Fl, floxed; gHE, global heterozygous; gHO, global homozygous; KO, knockout; PCR, polymerase chain reaction; WT, wild-type.

B. Immunofluorescence Staining and Microscopy

Immunofluorescence staining was performed as previously described [12]. Briefly, tissue cryosections or collected blastocysts at E3.5 were fixed in 4% paraformaldehyde, permeabilized with 0.1% triton X, blocked with 1% bovine serum albumin containing 1% donkey serum, and incubated in primary rabbit anti-TSPO monoclonal antibody (EPR5384) (ab109497; Abcam) [18] followed by secondary donkey antirabbit immunoglobulin G (H + L) antibody conjugated with Alexa Fluor 546 (Thermo Fisher) [19]. Nuclei were counterstained using UltraCruz aqueous mounting medium containing 4',6-diamidino-2-phenylindole (DAPI; Santa Cruz Biotechnology Inc). Microscopy was performed using Olympus FV1000 and Zeiss LSM 780 confocal laser scanning microscopes and an inverted Olympus microscope for epifluorescence imaging. All images were analyzed using ImageJ software (National Institutes of Health).

C. Preimplantation Embryo Collection

After gHE (*Tspo*$^{-/+}$) × gHE (*Tspo*$^{-/+}$) mouse pairings, the presence of vaginal plugs was checked the next day, and plug-positive females were euthanized on embryonic day E3.5. Blastocysts were collected by flushing the uterus as previously described (http://www.cellmigration.org/resource/komouse/komouse_protocols.shtml). Blastocysts were photographed and cultured in M16 medium (Sigma-Aldrich) for an additional day to observe their development. Abnormal morphology was recorded as previously described [20].

D. Oil Red O Staining

Male and female tissues of interest were embedded in optimum cutting temperature medium, and 6 μm cryosections were prepared at the histology core facility of the Goodman

Cancer Research Centre at McGill University. Frozen tissue sections were used for staining as recommended by the manufacturer (NovaUltra Oil Red O stain kit, IHC World). After staining, tissues were mounted with aqueous slide mounting medium for visualization. The staining of LDs were quantified using ImageJ software (NIH) following the procedures described previously [21].

E. Histochemistry and Transmission Electron Microscopy

For histochemistry testes were fixed in 4% paraformaldehyde. Paraffin-embedded testes from WT and *Tspo* gKO adult mice were prepared and sections stained with hematoxylin (Sigma-Aldrich) and eosin (Thermo Fisher Scientific) as previously described [22].

F. Transmission Electron Microscopy

For ultrastructural analyses, testis blocks were immersed in 5% glutaraldehyde overnight, post-fixed in cacodylate-buffered 1% osmium tetroxide, washed, dehydrated, and embedded in Epon resin [22]. Thereafter, samples were ultrathin-sectioned (~70 nm) and placed on grids. Electron microscopy was performed by the Doheny Eye Institute, using standardized procedures.

G. Blood Plasma Collection and Measurement of Circulating Steroids

We evaluated the activity of testes and adrenal glands in vivo by measuring levels of circulating testosterone and corticosterone, respectively. Blood was collected 6 days before euthanasia via submandibular puncture, and plasma was separated through centrifugation at 2000 × *g* for 15 minutes and stored at –80°C until used to determine steroid hormone levels. Enzyme-linked immunosorbent assay (ELISA)was used to measure testosterone and corticosterone (Cayman Chemicals) with intra-assay coefficients of variation (CV) of 8.8% and 6.2% respectively, as per the manufacturer's instructions. Absorbance was read at 420 nm using a VICTOR X5 Multilabel Plate Reader (PerkinElmer Inc).

H. Testicular Interstitial Fluid Collection

Using a 27-gauge needle, the tunica of the testes was punctured 3 to 4 times opposite the rete testis and centrifuged in a 1-mL pipet tip at 500 × *g* for 10 minutes. Interstitial fluid collected in the bottom of the tube was diluted in ELISA buffer (Cayman Chemicals) for testosterone measurement by ELISA.

I. Interstitial Leydig Cell Preparation

Interstitial cells were isolated from adult WT and *Tspo* gKO mice ranging in age from 56 to 97 days. Mice were asphyxiated with CO_2 and testes were removed. The tunica of the testis was removed, and seminiferous tubules were separated from interstitial cells by digestion (10 minutes, 34°C) in 0.25 mg/mL collagenase (Aldrich-Sigma)/13 mg/mL DNase (Aldrich-Sigma) in M-199 (Thermo Fisher Scientific) followed by unit-gravity sedimentation in M-199 supplemented with 1% bovine serum albumin [23]. Histochemical staining with nitro blue tetrazolium for 3βHSD activity with 0.4 mM etiocholanolone (Steraloids) as the steroid substrate [24] indicated the presence of an enriched Leydig cell population, containing 20% to 25% 3βHSD-positive cells. Cells were incubated at a concentration of 2.33×10^5 in a final volume of 1 mL for 2 hours in a shaking water bath at 34°C. Cells were incubated in buffered Dulbecco MEM:Ham F12 culture medium (Aldrich-Sigma) alone, or with a stimulating dose of 50 ng/mL human chorionic gonadotropin (hCG) (National Hormone Pituitary Program). Testosterone production was assayed by ELISA as described above.

J. Microarray Analysis and Data Mining

To analyze *Amhr2* and *Tspo* gene expression profiles during the preimplantation period of mouse embryo development, we retrieved the relevant raw data sets from gene arrays performed on different preimplantation stages of the mouse embryos (NCBI GEO: GSE18290 and GSE41358) [25, 26]. Data were further processed using FlexArray software (version 1.61; http://genomequebec.mcgill.ca/FlexArray) and normalized by robust multiarray average. The significance analysis of microarrays and analysis of variance (ANOVA) were used to select statistically significant altered genes with a P value equal to or less than .05. Volcano plots of mRNA expression from preimplantation stages were generated using FlexArray data. The data plotted along the x-axis were the means of $\log_2$-fold changes and along the y-axis were the negative logarithm of the P values.

K. RNA-Sequencing Data Analysis

Raw RNA-sequencing (RNA-seq) data for 8-cell and morula stages were retrieved from NCBI GEO (GSE44183) [27], and raw RNA-seq data for adrenal glands and lungs were retrieved from the National Center for Biotechnology Information Sequence Read Archive (SRP043599) and Gene Expression Omnibus (GSE84942), respectively [9, 28]. Data analysis was performed using an RNA-seq data analysis pipeline in the Galaxy platform (https://usegalaxy.org/) [29], following the instruction for the RNA-seq analysis pipeline. In brief, the original files with FASTQ format were loaded into the server and then aligned to the mouse genome (NCBI37/mm9) using Bowtie for Illumina, and graphing and display were performed using the UCSC Genome Browser (http://genome.ucsc.edu/) [30]. Data quantification and visualization were performed using SeqMonk built-in visualization tools (http://www.bioinformatics.babraham.ac.uk/projects/seqmonk/), including bp quantitation, and each gene was split into exons and normalized to a larger database from either the WT or HO data sets. At the same time, DESeq2 was used to verify the transcriptome changes after *Tspo* gene deletion. Mitochondrial proteins were retrieved from MitoCarta [31]. Cholesterol-binding proteins (411 proteins) that were selective for a trans-sterol probe over an N-palmitoylethanolamine structure (N-palmitoylethanolamine-diazirine-alkyne), but not sensitive to cholesterol competition, were retrieved from group III from a previously published proteome-wide mapping study [32]. Protein-protein interaction networks were retrieved from the STRING database (http://string-db.org) to provide information on global transcriptional response under *Tspo* deletion and were visualized using Cytoscape Network Analyzer (www.cytoscape.org).

L. Real-Time Polymerase Chain Reaction for Validation of RNA-Sequencing Data Analysis

Total RNA from mouse adrenal glands and lungs was extracted using TRIzol Reagent (Thermo Fisher Scientific). The values of 260:280 ratio and 260:230 ratio were 1.8 to 2.0 and 2.0 to 2.2, respectively, determined by a NanoDrop spectrophotometer and deemed acceptable for further analysis. All RNA samples were treated with DNA-free DNA Removal Kit (Thermo Fisher Scientific). RNA was subsequently diluted to 100 ng/μL using DNase/RNase-free water, and first-strand complementary DNA (cDNA) was then synthesized using the Transcriptor First-Strand cDNA Synthesis Kit (Roche Applied Science), according to the manufacturer's instructions with gene-specific primers (Table 1). The resulting cDNA samples were diluted with nuclease-free water and subjected to real-time PCR using SYBR green dye and a LightCycler 480 system (Roche Applied Science) as previously described [33]. The results reported for each RNA product were normalized to hypoxanthine-guanine phosphoribosyltransferase (*Hprt*) to correct for differences in the amounts of the template cDNA. The expression levels of each gene were further visualized within the whole RNA-seq data analysis in an MA-plot for reciprocal validation of the expression trend from the generated *Tspo* gKO mice.

M. Statistical Analysis

Statistical analyses were performed using GraphPad Prism 5.02 and 7.05 software. The significance of the results was determined using the Student t test or one-way ANOVA followed by the Bonferroni post hoc test for multiple comparisons. Chi-square test was performed using GraphPad QuickCalcs (http://graphpad.com/quickcalcs/chisquared1.cfm).

3. Results

A. Genetic Linkage Between Tspo *and Anti-Müllerian Hormone Type 2 Receptor-Cre*

We previously reported an unexpectedly small number of mice with a conditional homozygous floxed *Tspo* genotype (cHO: *Amhr2*-Cre$^{+/-}$, *Tspo*$^{fl/fl}$), but with a "WT-like" phenotype, where immunofluorescence staining of the testis showed normal TSPO expression [12]. These findings suggested it would be difficult to generate *Tspo* cKO mice using the *Amhr2*-Cre line, which is in contrast to the first report of a *Tspo* Leydig and Sertoli cell-specific cKO by Morohaku et al. [8]. A likely cause of the inconsistency may be due to the genetic linkage of *Tspo* and *Amhr2*-Cre genes on chromosome 15, which could hinder the generation of a cKO animal. Further examination of the issue showed that there is only a small chance of crossover-producing recombination between the *Tspo* and *Amhr2*-Cre genes, which depends on the distance between the 2 genes. Based on the genetic distance between *Tspo* and *Amhr2*, that is, 18.18 cM (1 cM = 0.01 recombinant rate) from the genetic map of Mouse Genome Informatics (http://www.informatics.jax.org/) [34] and using Haldane's map function and a controversial corrected Haldane's map function [35-37], there is approximately only a 7.62% to 9.0% (at least 7.62%) chance of cHO pups resulting from the pairing of a cHE mouse (*Amhr2*-Cre$^{+/-}$, *Tspo*$^{+/fl*}$) with a floxed *Tspo*-homozygous WT mouse (cHO: *Amhr2*-Cre$^{-/-}$, *Tspo*$^{fl/fl}$) (Fig. 1A). Because the small percentage of mice (4.4%) with cHO genotypes all have a WT-like phenotype [12], we assumed that either the Cre or the floxed allele(s) has a problem. Reanalysis of previously published microarray data on preimplantation embryos suggested that *Amhr2* is expressed as early as the 2-cell stage, suggesting that *Tspo* could be deleted at preimplantation embryonic stage(s) (Fig. 1B) [12]. Given that the cHE mouse used for the crossing carries a floxed allele (Fl*) of *Tspo* that passes through those early embryonic stages, but without targeting gene deletion, the Fl* would be a WT allele that could either be deleted in a tissue-specific manner, indicating the cHO genotypes are WT animals, or result in *Tspo* gHE mice (*Amhr2*-Cre$^{+/-}$, *Tspo*$^{-/fl*}$) if it carries one Fl* allele even after introducing a new functional floxed allele (Fig. 1A). This is the only way we can interpret why we could not replicate the paper by Morohaku and colleagues [8] and explain why the generated cHO mice exhibit "WT" phenotypes and no tissue-specific deletion of TSPO. All the redrawing of the breeding regimen is based on the fact that *Amhr2* is expressed during preimplantation embryo development as shown in microarray data reanalysis [12] and RNA-seq reanalysis (Fig.1B). Therefore, the *Amhr2*-Cre could not be used to produce a testis-specific *Tspo* cHO mouse, per se, as proved previously [12].

To provide experimental evidence on *Amhr2*-Cre activity at earlier preimplantation embryos, we investigated mice with a Rosa-mT/mG background (Fig.2A). Rosa-mT/mG mice express a double-fluorescent Cre-reporter in which the original expression of mT would be switched to that of mG with Cre activity [38]. At day 3 (E0.3.5) (or even at earlier stages) of preimplantation embryo development, *Amhr2*-Cre mediate recombination, where the CRE recombinase deletes a constitutively expressed mT transgene flanked by loxP sites (Fig. 2B). The mT is still switched into mG in certain areas, especially in the inner cell mass, of *Amhr2*-Cre$^{+/-}$; Rosa-mT/mG$^{+/-}$ blastocysts (Fig. 2C). In vitro cultured E4.5 embryos continue irreversibly to express the mG in the descendent cells with the recombined genotypes of half trophectoderm, in addition to the inner cell, in the embryos (Fig. 2C). This could be due to the asymmetric cell division for the first cell fate decision during preimplantation embryonic development [39]. The Cre-reporter

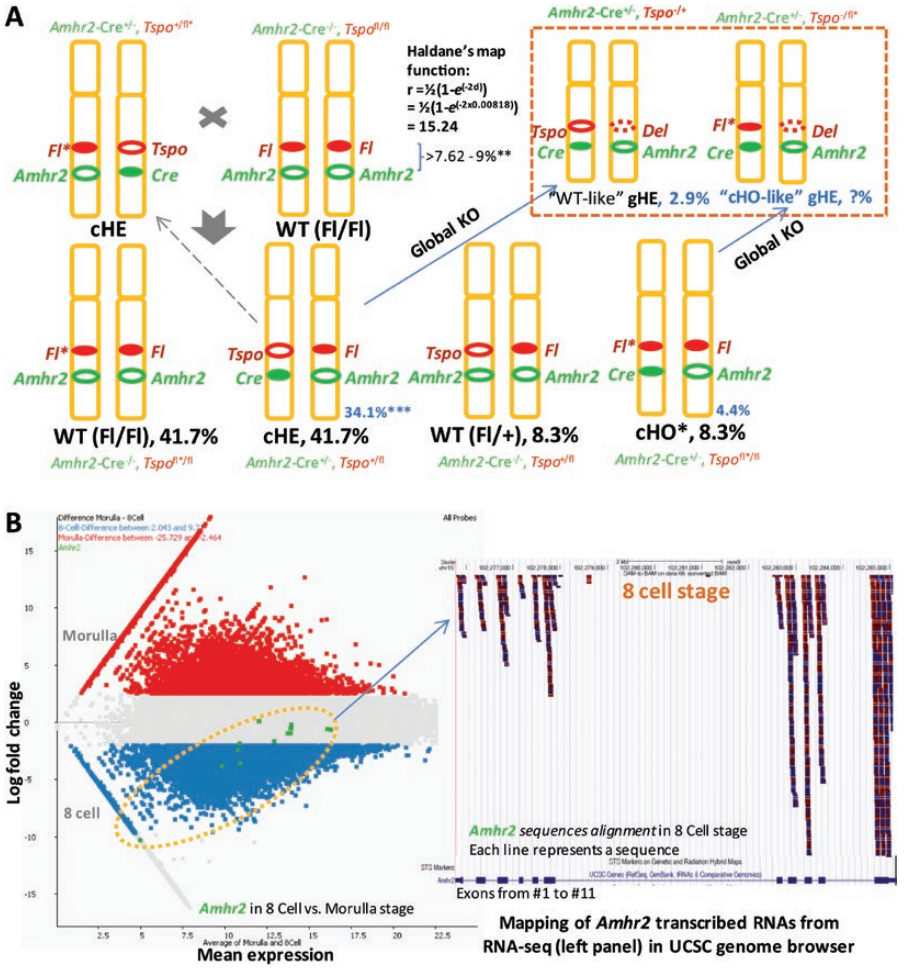

Figure 1. Genetic linkage between *Tspo* and anti-Müllerian hormone type 2 receptor-Cre (*Amhr2*-Cre) on chromosome 15 and *Amhr2*-mediated *Tspo* global knockout (gKO) (*Amhr2*-Cre$^{+/-}$, *Tspo*$^{-/+}$) and/or (*Amhr2*-Cre$^{+/-}$, *Tspo*$^{-/fl*}$). A, Breeding scheme originally used in our previous experiments [12], expected chromosomal crossover (8.3%), and the likelihood of *Tspo* gKO leading to a genotype switch. Some conditional heterozygous (cHE) genotypes switched to a "wild-type (WT)-like" with one allele globally deleted (global heterozygous [gHE]), and some conditional homozygous (cHO) genotypes remained HO genotypes but with one allele globally deleted ("cHO-like" gHE); therefore, the cHO genotype includes both cHO and gHE. Fl* is a "defective" floxed *Tspo* allele, because it passes by the embryo stage without targeting a deletion, leading to a cHO* that has actually a WT allele. cHE and cHO both contain a WT *Tspo* allele coming either from Fl* or newly introduced, indicated by a light-color dotted arrow back to the original cHE parents. All numbers indicated as percentages are expected proportions except the blue numbers: 34.2% of cHE, 4.4% cHO, and 2.9% value of "WT-like" gHE, which were observed from our crossing experiments for the conditional knockout (cKO) breeding scheme. Haldane's map function is shown, and the recombination frequency between *Amhr2* and *Tspo* was estimated to be no more than 7.62%. *Indicates the "defect floxed allele" during cKO genotyping where the *Amhr2*-Cre does not work at the early embryo development, so the cHO* actually has a WT allele of *Tspo* all the time with a final mixed genotyping of cHO and gHE. In this report, the 2 gHE mice were crossed to produce a gHO mouse analyzed in Fig. 3. Percentages of the observed ratios are indicated in blue. **The recombination rate was estimated based on Haldane's and Casares' map function. Abbreviations: r, recombination rate; d, genetic distance in Morgans. ***Newly introduced "defect floxed allele." B, *Amhr2* is expressed at 8-cell stage of preimplantation embryo. RNA-sequencing data were retrieved from NCBI GEO (GSE44183) [27] and reanalyzed using the Galaxy platform [29], then visualized using SeqMonk built-in visualization tools and in the UCSC Genome Bowser (https://genome.ucsc.edu/) [30]. Each exon is shown as in an MA-plot for the whole set of sequences (right) and also in the Genome Browser sequence alignments (left) from exon(s) 1 to 11 (left).

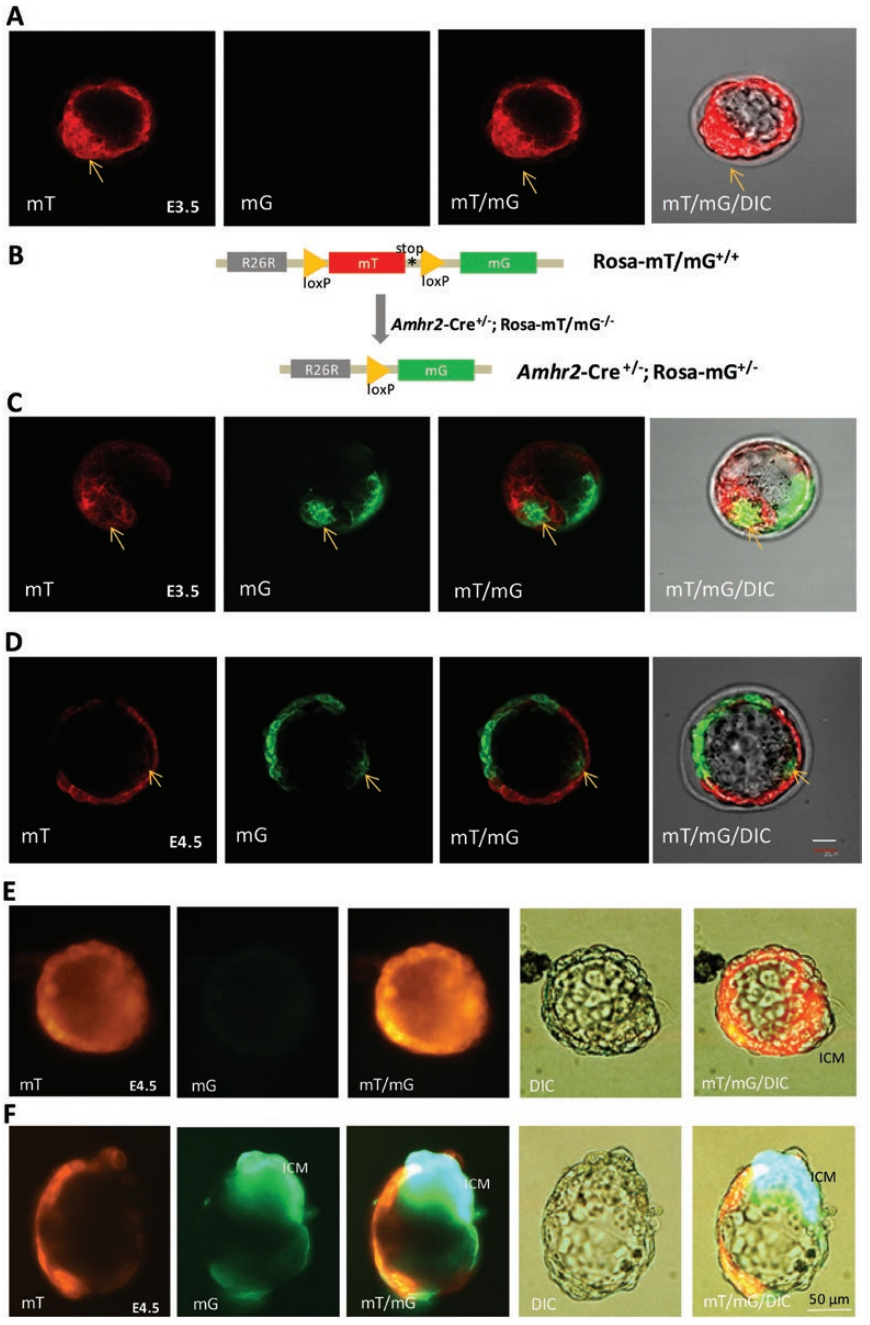

Figure 2. The specificity and efficiency of anti-Müllerian hormone type 2 receptor-Cre (*Amhr2*-Cre)–mediated recombination were determined using Rosa-mT/mG$^{(+/-)}$ reporter mice. A, The E3.5 whole blastocysts were from Rosa-mT/mG$^{+/+}$ mice. The images from 3 channels: red (mT, Tomato red), green (mG, membrane GFP), and differential interference contrast (DIC) were collected and overlaid using an Olympus FLUOVIEW FV1000 confocal laser scanning microscope. B, Diagram of the strategy used to assess the degree of preimplantation embryo-specific recombination. *Amhr2*-Cre mice were crossed to Gt(ROSA)26Sort$^{m4(ACTB-tdTomato,-EGFP)Luo}$ reporter mice. These reporter mice ubiquitously express mT, A, before Cre activation and C and D, mG on Cre activation, as evaluated by confocal laser scanning microscope. C, Whole blastocysts view of E3.5 from *Amhr2*-Cre$^{(+/-)}$; Rosa-mT/mG$^{(+/-)}$ mice with dual detection of mT (red) and mG (green) fluorescence. D, View of the same blastocysts at E4.5 *Amhr2*-Cre$^{+/-}$; Rosa-mT/mG$^{+/-}$ mice after in vitro culture overnight. Arrow, inner cell mass (ICM) where the recombination occurs. Scale bars = 20 µm. E, Epifluorescence view of whole blastocysts at E4.5 from Rosa-mT/mG$^{+/+}$ mice after in vitro culture overnight (as shown in A). F, Epifluorescence view of whole blastocysts at E4.5 from Amhr2-Cre$^{+/-}$; Rosa-mT/mG$^{+/-}$ mice after in vitro culture overnight (as shown in D). Scale bar, 50 µm.

was actively expressed primarily in the central part of the inner cell mass, indicating that the gene knockout occurs early in the primordial embryo. These conclusions were further confirmed by epifluorescence microscopy (Fig.2E and 2F).

Thus, the *Amhr2*-Cre$^{+/-}$ mouse serves as a "global deleter" instead of conditional, which is consistent with our findings from bioinformatic analysis of *Amhr2* gene expression at preimplantation embryos. This finding suggests it may be necessary to reinterpret any previous data on *Amhr2*-Cre–conditional KO gene deletion, including the *Tspo* gene.

B. Anti-Müllerian Hormone Type 2 Receptor-Cre–Mediated Global Tspo *Deletion*

As shown in Fig. 1, mice of "WT-like" gHE genotype (*Amhr2*-Cre$^{+/-}$, *Tspo*$^{-/+}$) from the expected cHE (*Amhr2*-Cre$^{+/-}$, *Tspo*$^{+/fl*)}$ were used to cross with WT (C57BL/6J) animals to produce gHE mice (*Tspo*$^{-/+}$); crossing of 2 gHE (*Tspo*$^{-+}$) will produce gHO (*Tspo*$^{-/-}$; gKO) mice (Fig. 3A shows PCR genotyping and sequencing data demonstrating the presence of [left panel] "WT-like" gHE [*Amhr2*-Cre$^{+/-}$, *Tspo*$^{-/+}$] , cHO mice [*Tspo*$^{+/+}$, *Tspo*$^{-/+}$] from gHE crossed with [middle panel] WT [C57BL/6J] mice, and [right panel]gHO [gKO] generated from the crossing of 2 gHE (*Tspo*$^{-/+}$) mice). Global deletion of the *Tspo* gene is confirmed by sequencing the targeted region of the *Tspo* locus and PCR using mouse tail snips and the primer sets: gKO-F/gKO-R in gKO (*Tspo*$^{-/+}$ and/or *Tspo*$^{-/-}$) mice after exon 2 and exon 3 deletion (196 bp) and exon2-RR/exon2-FF in WT (*Tspo*$^{+/+}$) mice (300 bp).

To further examine the reason behind this observation, we reanalyzed previously published microarray data sets (GSE18290) of mouse embryo *Tspo* expression profiles at 1-cell, 2-cell, 4-cell, 8-cell, morula, and blastocyst stages [12, 26]. We found that *Amhr2* was predominately expressed during the 2- to 8-cell stages, whereas *Tspo* was predominately expressed during morula and blastocyst stages (1-way ANOVA, $F_{(5,12)} = 5.588$, $P < .01$, $n = 3$). Reanalysis of another data set (GSE41358) of mouse preimplantation in vitro fertilized embryos showed that *Amhr2* expression decreased during the blastocyst stage, whereas *Tspo* expression increased during the blastocyst stage (one-way ANOVA, $F_{(4,10)} = 25.98$, $P < 0.001$, $n = 3$; 3 probes per gene; Fig. 3B and 3C) [25]. Further immunofluorescence staining of TSPO in blastocysts at E3.5 indicates that TSPO is strongly expressed at this stage (Fig. 3D). These results provide a theoretical basis to support the *Amhr2*-Cre–mediated generation of a *Tspo* gKO but not cKO, and show that TSPO plays a role in normal mouse preimplantation embryo development.

C. Confirmation of Anti-Müllerian Hormone Type 2 Receptor-Cre–Mediated Tspo *Global Knockout*

TSPO expression in adult WT (*Tspo*$^{+/+}$), gHE (*Tspo*$^{+/-}$), and gHO (*Tspo*$^{-/-}$), mice were investigated by indirect immunofluorescence staining and confocal microscopy. Strong TSPO staining was observed in Leydig cells in WT mice, whereas TSPO staining was weaker in gHE mice and not observed in gHO mice (Fig. 4A-4F). Similar expression patterns were observed using both confocal and epifluorescence microscopy. In adrenal glands, TSPO was strongly expressed in the cortex area of WT mice, whereas it was weakly expressed in the cortex area of gHE mice and not expressed in the cortex area of gHO mice (Fig. 4G-4L). Moreover, strong staining was observed in the fat tissue around WT adrenal glands, but no staining was observed in the fat tissue around gHO adrenal glands.

Immunofluorescence staining of other tissues showed that TSPO was absent in gHO mice and weakly present in gHE mice compared with WT mice based on both confocal and epifluorescence microscopy. In the WT mouse brain, TSPO immunostaining was seen as sparsely distributed spots (Fig. 5A, 5B, 5D, 5E, 5G, and 5H), which are likely to be localized in microglia and endothelial cells as shown in several previous reports [12, 40-43]. In the gHO brain, there was no expression of TSPO, indicating that the staining in brain is TSPO specific (Fig. 5C, 5F, and 5I). In addition, TSPO was completely absent in the liver of gHO mice, but was weakly expressed in gHE mice and highly expressed in WT mice (Fig. 5J-5O).

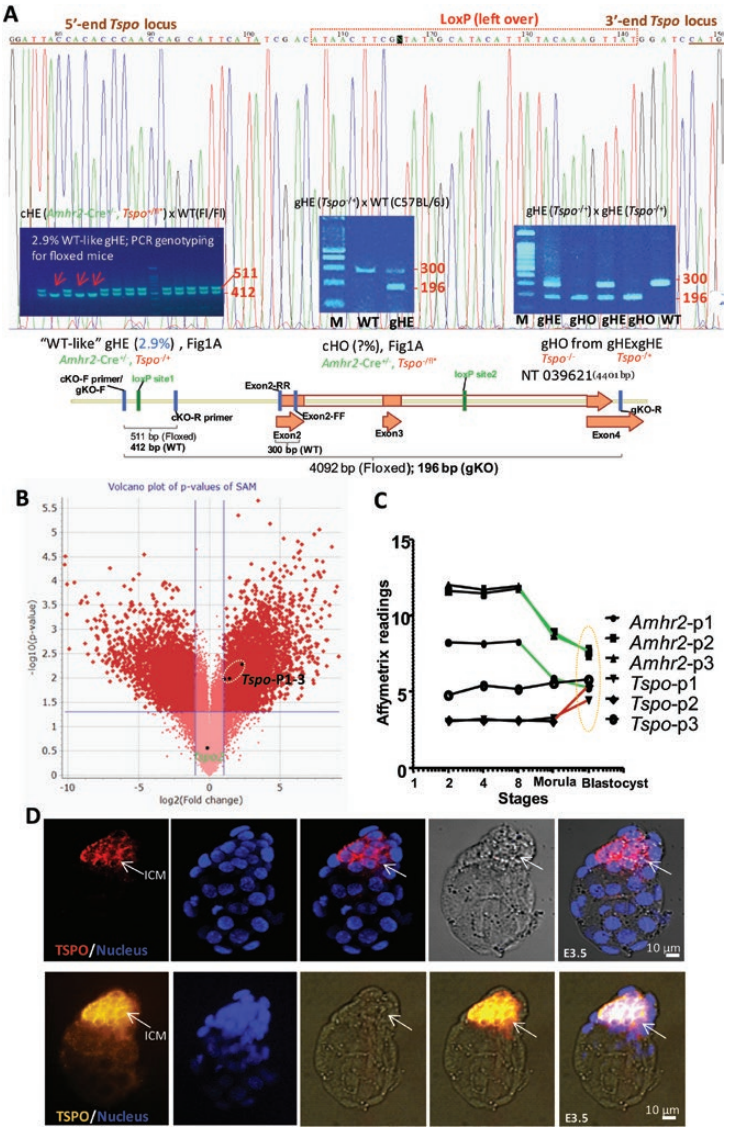

Figure 3. Anti-Müllerian hormone type 2 receptor-Cre (*Amhr2*-Cre)–mediated global *Tspo* deletion ($Tspo^{-/-}$) and timing of *Amhr2* and *Tspo* expression during embryonic development. A, *Amhr2*-Cre–mediated global *Tspo* knockout (KO) confirmed by polymerase chain reaction genotyping and sequencing of mouse tail snips. Approximately 2.9% of mice used in the experiments had a "wild-type (WT)-like" gHE (*Amhr2*-$Cre^{+/-}$, $Tspo^{-/+}$), indicating that *Tspo* was deleted globally in Cre-positive mice. Red arrows in the agarose gel used for genotyping: indels, from left to right, show the rare unexpected genotype, regenotyping of the last selected conditional homozygous (cHO) using gene deletion–specific primer to identify global heterozygous (gHE), and global homozygous (gHO) ($Tspo^{-/-}$) produced by gHE × gHE crossings. The band sizes used for identification of WT and KO are indicated. M: 100 bp ladder. Primers used are indicated in the diagram below sequencing chromatography. **B**, Volcano plot of expression values between the 2-cell and blastocyst stages, with *Tspo* and *Tspo2* shown as black dots. C, Expression profiles of *Amhr2* and *Tspo* were obtained from 3 probes for each gene during preimplantation embryonic development of in vitro fertilized mouse embryos. Significant changes between stages are highlighted in red (increased) and green (decreased). The dotted orange circle highlights the increased Tspo expression at blastocyst stage. D, Immunofluorescence staining of translocator protein (TSPO) in mouse blastocyst at E3.5. Representative images show that localization of TSPO was in the inner cell mass (ICM) (indicated by arrow) with anti-TSPO antibody (red for confocal imaging, yellow for epifluoresence). Nuclei were stained with 4',6-diamidino-2-phenylindole (DAPI) (blue). Differential interference contrast images were used as controls. Top panels: laser scanning confocal microscopy images; low panels: epifluorescence microscopy images. Scale bar represents 10 µm.

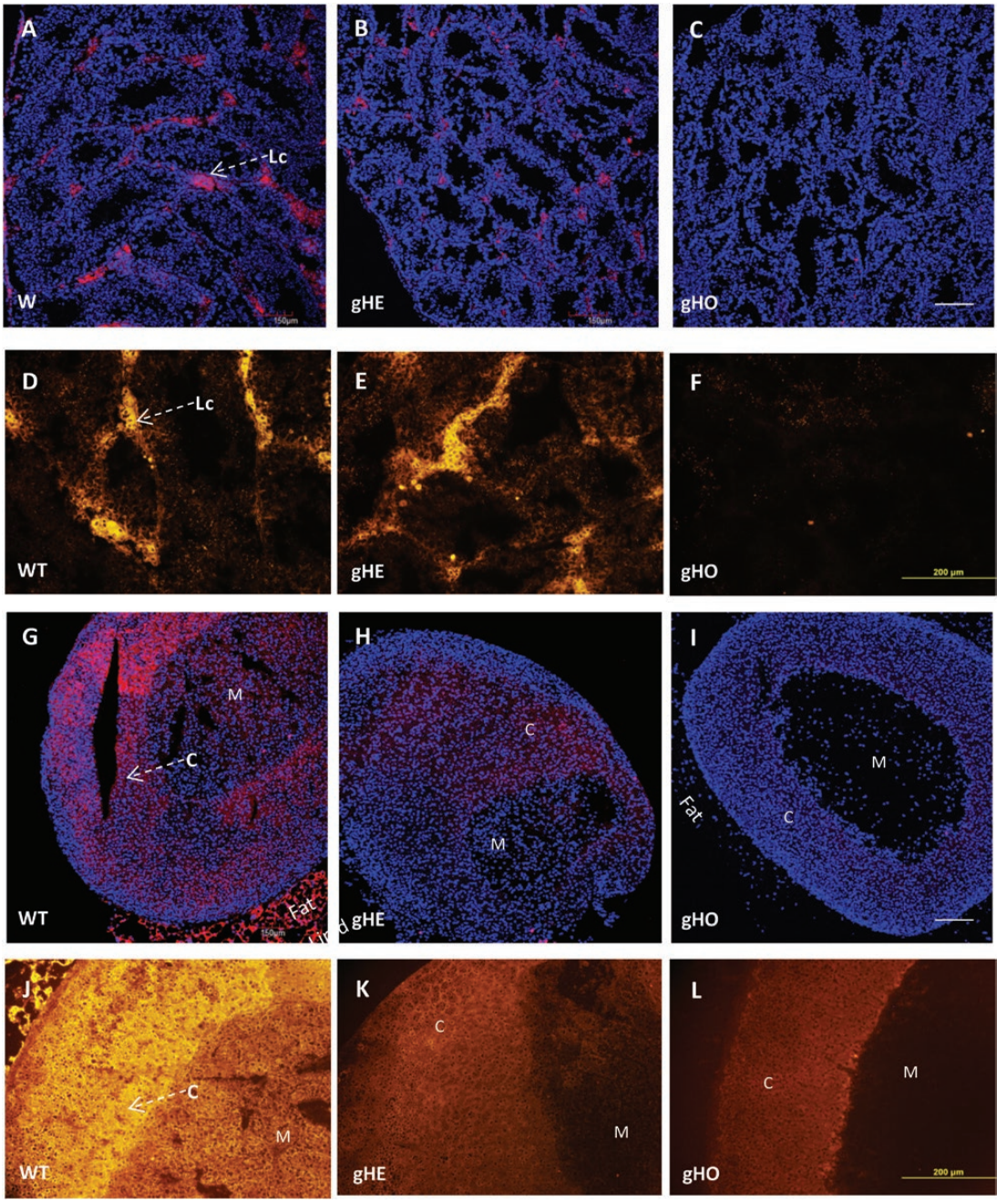

Figure 4. Immunofluorescence staining of translocator protein (TSPO) in the testis and adrenal gland of wild-type (WT) (*Tspo*$^{+/+}$), global heterozygous (gHE) (*Tspo*$^{+/-}$), and global homozygous gHO (*Tspo*$^{-/-}$) mice. A to C, Representative confocal fluorescence images of TSPO staining (anti-TSPO antibodies [Ab], red) and nuclei counterstaining (4',6-diamidino-2-phenylindole [DAPI], blue) and D to F, epifluorescence microscopy images of TSPO staining (anti-TSPO Ab, orange) in the testis. Representative G to I, confocal fluorescence images of TSPO staining (anti-TSPO Ab, red) and nuclei counterstaining (DAPI, blue) and J to L, epifluorescence microscopy images of TSPO staining (anti-TSPO Ab, orange) in the adrenal gland. Abbreviations: C, cortex; M, medulla; Lc, Leydig cell. Scale bar, 200 µm.

Taken together, we believe these results suggest that *Tspo* was globally deleted as we expected from genotyping of the mice, microarray data analysis, and the cell membrane-targeted, 2-color fluorescent Cre-reporter (Rosa mT/mG) analysis.

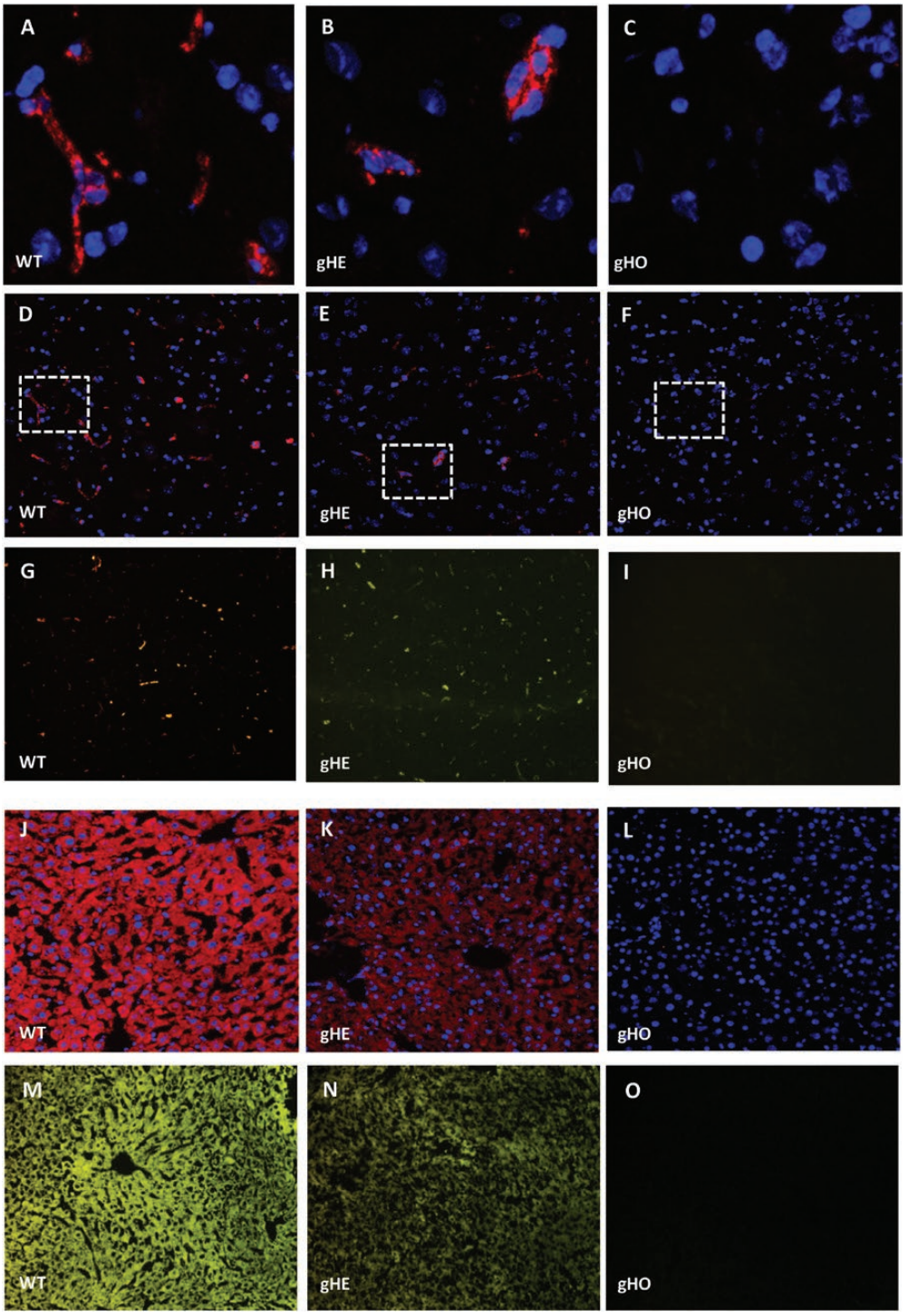

Figure 5. Immunofluorescence staining of translocator protein (TSPO) in the brain and liver of wild-type (WT) (*Tspo*$^{+/+}$), global heterozygous (gHE) (*Tspo*$^{+/-}$), and global homozygous (gHO (*Tspo*$^{-/-}$) mice. A to C, Representative confocal fluorescence images of TSPO staining (anti-TSPO antibodies [Ab], red) and nuclei counterstaining (4',6-diamidino-2-phenylindole [DAPI], blue) within the D to F, highlighted areas and G to I, epifluorescence microscopy images of TSPO staining (anti-TSPO Ab, orange) in the brain. Representative J to L, confocal fluorescence images of TSPO staining (anti-TSPO Ab, red) and nuclei counterstaining (DAPI, blue) and M to O, epifluorescence microscopy images of TSPO staining (anti-TSPO Ab, orange) in the liver. Scale bar, 200 μm.

D. Adverse Effect of Global Tspo *Deletion on Preimplantation Embryo Development*

We previously reported that there were no morphological changes at E12.5 of "gKO" mice but observed lower than expected proportions of certain genotypes at birth [12]. Thus, we performed a closer examination of preimplantation embryonic stages to detect potential abnormalities in development. Indeed, we found that 33.3% of blastocysts at E3.5 to 4.5 had a normal morphology (Fig. 6A), whereas 66.7% showed delayed development (Fig. 6B), which are close to the expected proportions of 25% of WT (*Tspo*$^{+/+}$) and 75% of HE and HO *Tspo*$^{-/-}$ 25%; *Tspo*$^{+/-}$ 50% mice. These results are in contrast to 95% to 99% of WT (*Tspo*$^{+/+}$) blastocysts obtained from mice produced from the pairing of *Tspo*$^{+/+}$; *Amhr2*-Cre$^{+/-}$ with *Tspo*$^{+/+}$; Rosa-mT/mG$^{+/+}$ mice, which showed normal development in vitro (Fig. 6C) [44]. These results are consistent with a previous report of low TSPO expression in fragmented or apoptotic preimplantation embryos with associated lipid accumulation [20], as well as with our gene expression profiling showing increased *Tspo* expression during blastocyst development (Fig. 3B, 3C, and 3D). It is clear then that TSPO is needed for normal preimplantation embryo development.

E. Changes in Neutral Lipid Storage After Global TSPO *Depletion*

Neutral lipids, including dominant esterified cholesterol in steroidogenic and/or TSPO-rich tissues, are the source of cholesterol for steroid biosynthesis [45]. We evaluated the presence of LDs enriched with esterified cholesterol from these tissues, including the testis, adrenal gland, liver, and ovary. After TSPO depletion, we found decreased neutral lipids in the testis (Fig. 7A-7C) and increased neutral lipids in the adrenal gland (Fig.7D-7F), liver (Fig. 7G-7I), and ovary (Fig. 7J-7L). Similar patterns of lipid accumulation in the testis, adrenal gland, and ovary were previously observed in *Nr5a1*-Cre–mediated *Tspo* cKO mice in a tissue-specific manner and were accompanied by a lack of corticosterone production in response to ACTH [12]. The accumulation of neutral lipids is a sign of changes in the use of cholesterol as the substrate of steroid biosynthesis, while in parallel preventing the accumulation of excess toxic free cholesterol, in agreement with previous reports for either *Tspo* [12, 14] or *Star* [13].

F. Steroid Biosynthesis After Global TSPO *Depletion*

We measured circulating testosterone and corticosterone levels to assess the steroidogenic capacity of the testes and adrenal glands of *Tspo* gKO mice. We found that *Tspo* gHE and *Tspo* gHO mice showed significantly lower testosterone levels than WT mice ($P < .05$; Fig. 8A), whereas there was no difference in basal corticosterone levels between WT, gHE, and gHO mice (Fig. 8B), in agreement with previous results on a mouse cKO [12] as well as the recent data on *Tspo*-mutant rat lines [14]. The constant or changed steroid levels in these steroidogenic tissues may reflect the physical condition(s) of mitochondria under TSPO deficiency, as well as the availability of free cholesterol from different sources. Indeed, indirect evidence of accumulation of lipids in adrenal glands could reflect the upregulated *Aup1* gene (Fig. 8C), which is an LD regulating VLDL assembly factor; high expression of this gene results in increased LD clustering [46, 47].

To further assess the impact of TSPO deficiency on testosterone production, we measured intratesticular testosterone levels in WT and *Tspo* gKO mice. Data obtained are presented as percentage of WT. Considering that we observed a slight but significant increase in *Tspo* gKO testis weight (Fig. S1) [48], the data were corrected per gram of testis weight. A significant 53% reduction in intratesticular testosterone levels was seen in *Tspo* gKO mice ($P < .05$; Fig. 9 left). These results were consistent with results obtained using enriched interstitial Leydig cell preparations isolated from WT and gKO mice (Fig. 9). Cells isolated from WT animals showed a 3-fold stimulation of testosterone production in response to saturating concentrations of hCG, whereas cells isolated from *Tspo* gKO mice failed to

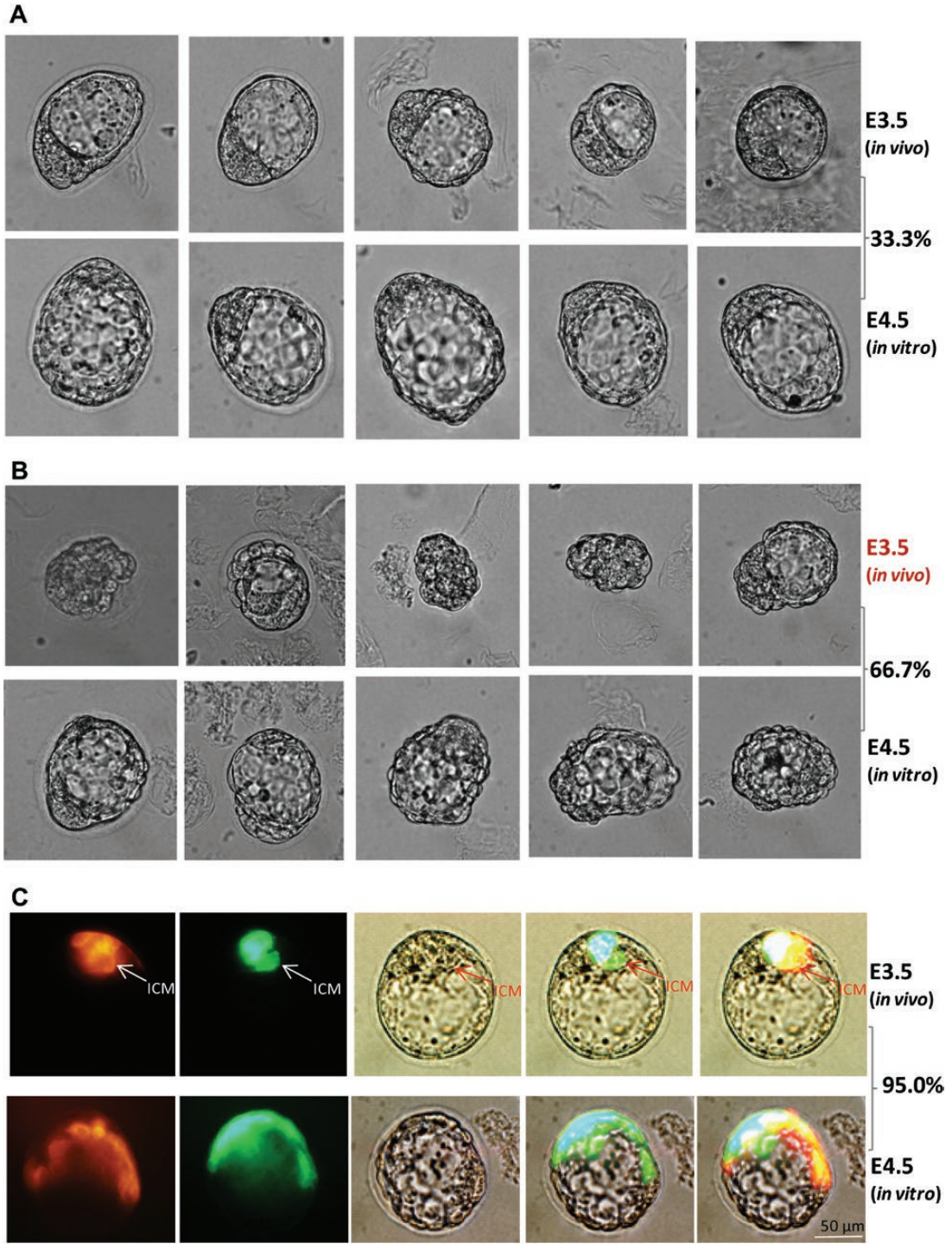

Figure 6. Morphology of blastocysts from anti-Müllerian hormone type 2 receptor-Cre (*Amhr2*-Cre)–mediated *Tspo* global heterozygous (gHE) (*Tspo*$^{+/-}$) × gHE (*Tspo*$^{+/-}$) pairings. Representative images of preimplantation embryos at E3.5 (in vivo, n = 30 checked in total; upper panel) and E4.5 (in vitro cultured overnight, n = 30 checked in total; lower panel). A, One-third had a normal morphology, whereas B, two-thirds showed delayed development at E0.3.5. **C**, Morphology of blastocysts from wild-type pairings (*Tspo*$^{+/+}$; *Amhr2*-Cre$^{+/-}$ with *Tspo*$^{+/+}$;Rosa-mT/mG$^{+/+}$). A representative blastocyst is shown with *Tspo*$^{+/+}$; *Amhr2*-Cre$^{+/-}$; Rosa-mG$^{+/-}$ genotype, where 95% have a normal morphology at E0.3.5 (n = 21). Scale bars = 50 µm.

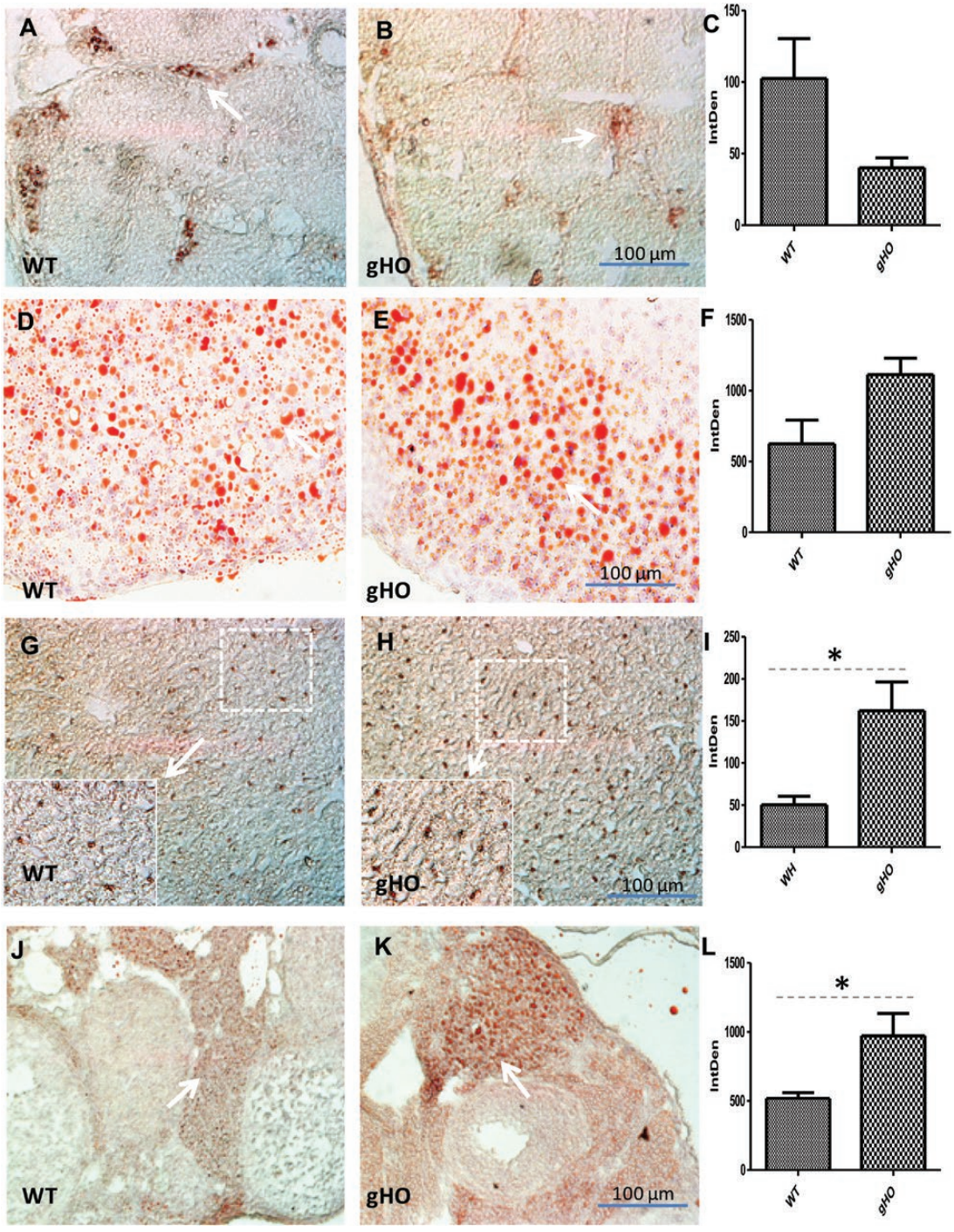

Figure 7. Comparison of neutral lipid storage in testis, adrenal gland, liver, and ovary after anti-Müllerian hormone type 2 receptor-Cre (*Amhre*-Cre)–mediated translocator protein (TSPO) depletion. Representative images of Oil Red O staining showing lipid droplets (LDs) in the WT (*Tspo*$^{+/+}$) vs global homozygous (gHO) (*Tspo*$^{-/-}$) A to C, testis; D to F, adrenal gland; G to I, liver; and J-L, ovary. C, F, I, and L, quantification of the staining of LDs from 4 to 5 individual animals. Student t test (testis: $P = .05$; adrenal gland: $P = .05$; liver: $P = .01$; ovary: $P = .03$). Data are presented as means ± SEM; n = 6 animals per group. *P less than .05. Scale bar, 100 µm. White arrow highlights LD-stained areas.

respond to hCG. No differences were observed in seminal vesicle, epididymis, kidney, and whole-body weights (Fig. S1) [48]. Histochemical analysis of testis sections failed to show any major morphological differences in testes from WT and *Tspo* gKO mice (Fig. S1) [48].

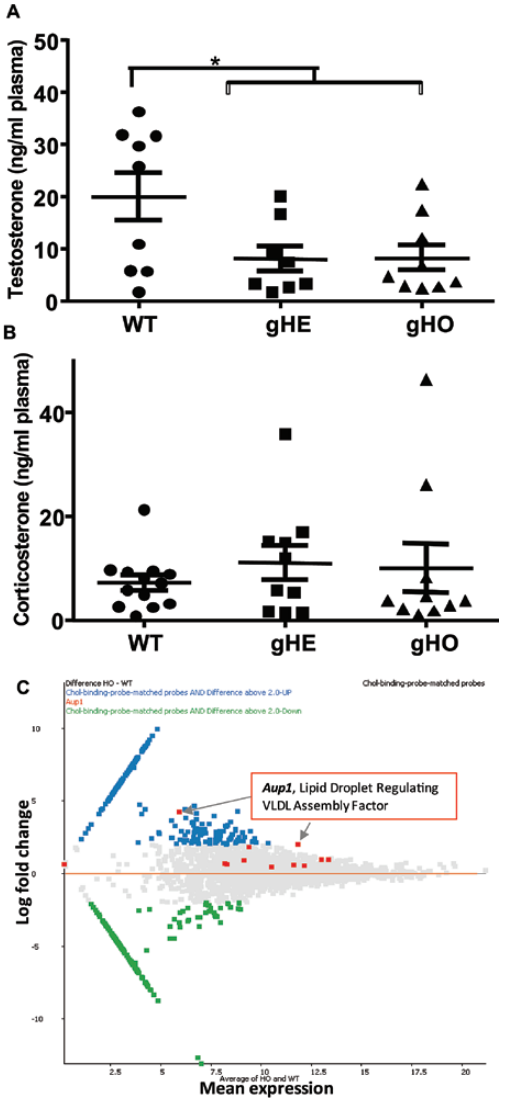

Figure 8. Circulating A, testosterone and B, corticosterone levels in the plasma of wild-type (WT) (*Tspo*$^{+/+}$), global heterozygous (gHE) (*Tspo*$^{+/-}$), and global homozygous (gHO) (*Tspo*$^{-/-}$) mice. **P* less than .05, Mann-Whitney U tests (data presented as means ± SEM; n = 8-12 animals per group). C, Elevated gene expression of ancient ubiquitous protein 1 (*Aup1*), a lipid droplet regulating VLDL assembly factor, in mouse adrenal glands (WT vs global knockout). Blue and green spots represent each exon of the cholesterol-binding genes. Red spots represent exons of the *Aup1* gene.

Transmission electron microscopy studies were undertaken to assess Leydig cell ultrastructure in WT and *Tspo* gKO mice. No significant differences were seen in Leydig cell morphology between WT and *Tspo* gKO mice (Fig. 10A-10D), except that Leydig cells from *Tspo* gKO mice contained autophagosomes that we rarely observed in WT mice (Fig. 10E-10F).

G. TSPO *Depletion Leads to Global Transcriptional Changes Related to Protein Relocalization, Mitochondrial Ion Transport, and Proton Leak Pathways*

Because TSPO is needed for the development of preimplantation embryos and adult steroid biosynthesis, the inconsistent results on the roles of TSPO from previous reports [8, 12, 14, 28] might involve a compensatory mechanism, which is likely to be established in the early preimplantation period of embryogenesis under TSPO deficiency, when survival selection

for cell fate decisions has begun via genetic network rewiring. Indeed, 2 previous reports propose that compensation occurs after deleterious mutation via gene or network replacement, but that it does not occur after a gene knockdown [49, 50]. Therefore, we sought to identify the mechanism behind this possible compensation to ultimately increase our understanding of steroidogenesis in animals.

We reanalyzed 2 sets of raw RNA-seq data associated with studies showing that TSPO depletion did not affect gene expression profiles [9, 28]. *Tspo*-deleted and nondeleted exons of

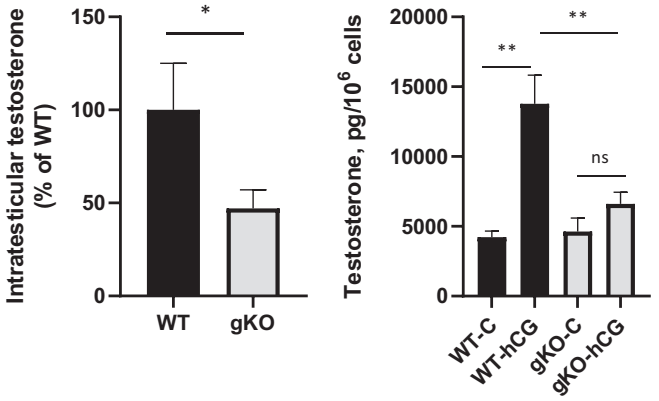

Figure 9. Left panel. Intratesticular testosterone levels in wild-type (WT) (*Tspo*$^{+/+}$) and global homozygous (gHO) (*Tspo*$^{-/-}$) mice. Data are presented as means ± SEM; n = 13 to 14 animals per group; **P* less than .05. Intratesticular testosterone levels in WT animals were on average 50 ng/g per testis. Right panel. Testosterone formation by isolated Leydig cells in response to 50 ng/mL human chorionic gonadotropin (hCG). Results shown are from n = 4 (WT), n = 7 (global knockout [gKO] control), and n = 5 (gKO hCG) animals. Data shown are the mean ± SEM. **, *P* less than .01 compared to controls. Abbreviation: ns, nonsignificant.

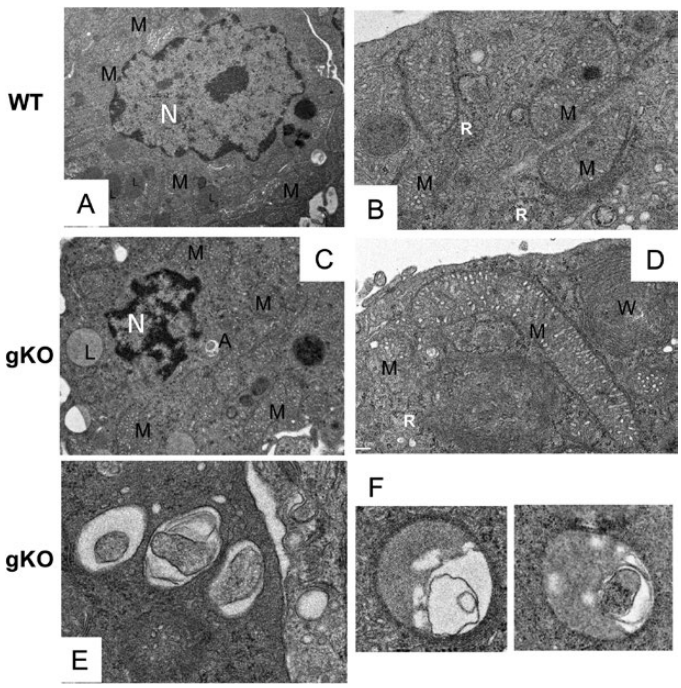

Figure 10. Transmission electron microscopy images showing the ultrastructure of A and B, wild-type (WT) (*Tspo*$^{+/+}$) and C and D, global knockout (gKO) (global homozygous [gHO], *Tspo*$^{-/-}$) Leydig cells. E and F show autophagosomes identified in gKO (gHO, *Tspo*$^{-/-}$) Leydig cells. Abbreviations: LDs, lipid droplets; M, mitochondria; N, nucleus; W, swirled variety of smooth endoplasmic reticulum.

the gene were used as negative and positive controls, respectively, and the relevant graphs were visualized using UCSC Genome Browser under custom tracks. By viewing scatter plots of WT vs *Tspo* deletion (gHO), we selected genes that were uniquely upregulated (red) or downregulated (green) in the adrenal gland (Fig.11A) and lung (Fig. 11B; Tables S1-S4) [48], with the dashed circle (purple) indicating genes that were specifically downregulated in the lung (Fig. 11B; Table S5) [48]. Corresponding loci for the selected genes, including *Tspo*, *Ucp2*, *Fdxr*, *Krt78*, *Krt5*, and *Caps4*, are shown to indicate the differential sequence alignment(s) (Figs. S3, S4, and S9-S11) [48]. Additionally, the clustering of gene expression profiles and the upregulated and downregulated gene networks likely indicate functional compensation after TSPO depletion (Figs. S5-S7 and S11-S13) [48].

Of the 4 major players in steroidogenesis, *Cyp11a1*, *Star*, *Vdac1*, and *Tspo, Star* had slightly lower expression and *Cyp11a1* had higher expression in gHO adrenal glands compared with WT adrenal glands (Fig. 11C), in agreement with previous real-time PCR results [9], whereas there were no noticeable changes in the same genes in the lung (Fig.11D). In cross-comparison with mitochondrial cholesterol–binding proteins, scatter and volcano plots suggest several genes are likely to replace TSPO functionally as an outer mitochondrial membrane cholesterol–binding protein (Figs. 11E and 11F, S7 and S13). To further illustrate the positive changes of mitochondrial cholesterol–binding protein-encoding genes, *Ucp2* and *Fdxr* genes were both retrieved for analysis, instead of exons, as the basic unit (Fig. S4) [48]; genes in a mitochondrial protein interaction network are highlighted (colored) (Fig. 12). Interestingly, one of the upregulated genes, the *Apoo* gene that encodes 3 isoforms (mitochondrial form Iso1, partial mitochondrial form Iso2, and nonmitochondrial form Iso3), is related to differential pre-messenger RNA (mRNA)-splicing of exon 1, whereas the rest of the genes are involved in ion transport or proton leak associated with mitochondrial membrane potential, which likely reflects the basic role of TSPO conserved across cells, tissues, and species [51]. To cross-compare with the data from previous RNA-seq analyses, we present selected genes from DESeq2 analysis (Fig. S14; Table S6), which is consistent with a previous report [9].

To validate the reanalysis of RNA-seq data, we performed real-time PCR and RNA-seq data visualization in a genome browser (Figs. S3-S13). Several important genes were selected among upregulated and downregulated gene sets to confirm whether their expression levels were increased or decreased in the adrenal glands of the *Amhr2*-Cre–mediated *Tspo* gHO mice using real-time PCR (Fig. 13). Real-time PCR confirmed the increased expression levels of *Abcb6*, *Ucp1*, *Ucp2*, and *Apoo* in *Tspo* gHO mice but not that of *Trp53imp2* (Fig. 13A-13D). Real-time PCR also confirmed the reduced expression of *Nr4a2* and *Trim5* in the *Tspo* gHO mice, although there was great variability (Fig. 13E and 13F). Each exon of the investigated genes was mapped to an MA-plot of the RNA-seq data (Fig. 13G). *Hprt* was used as the reference gene in the real-time PCR and is found around the central line. The upregulated genes *Ucp1* and *Ucp2* in red are above the line, and the downregulated gene *Nr4a2* is below the central line. Each coding exon of *Tspo* is shown as the control: Exon2 and exon3 are down to the edge of the dot distribution and exon4 is below the central line (Figs. 11G; S3 and S8) [48]. UCP1 and UCP2 are both required for mitochondrial proton leak (Fig. 13H).

The transcriptome profiling changes and especially the expression levels of several specific genes, verified from real-time PCR, show that compensation for TSPO deficiency took place. This likely involves mitochondrial membrane potential via changes between inner and outer mitochondrial membrane contact through the mitochondrial contact site complex and cholesterol transport from Golgi vesicles [51, 53, 54].

4. Discussion

Amhr2-Cre was first reported to mediate the targeted disruption of the widely expressed type I bone morphogenetic protein (BMP) receptor *Bmpr1a* (also known as *Alk3*) in *Amhr2-Cre*–knockin mice, where the Cre replaced one allele of the *Amhr2* gene [55]. Since then,

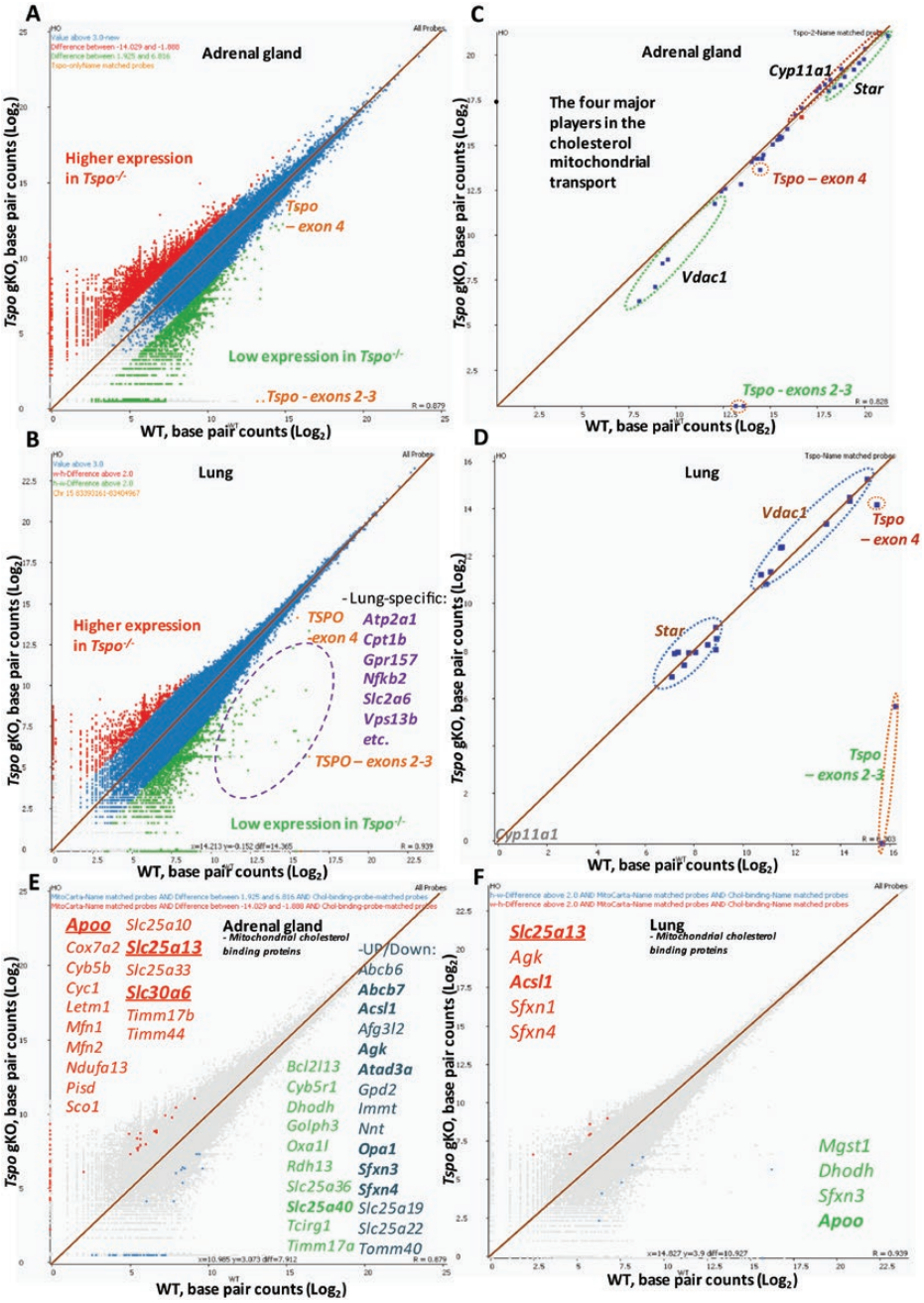

Figure 11. Whole-genome transcript profiling to identify differentially expressed genes associated with translocator protein (TSPO) depletion in mouse adrenal glands and lungs: reanalysis of 2 previously published sets of RNA-sequencing (RNA-seq) data [9, 28]. Scatter plot of RNA-seq data from A, adrenal glands and B, lungs. Red dots: high expression, green dots: low expression (including *Tspo* as a positive [exon 4] or negative [exons 2/3] control). Scatter plots for C, adrenal glands and D, lungs showing 4 major players in steroidogenesis: *Cyp11a1, Star, Vdac1,* and *Tspo*. Red dotted circle: high expression, green dotted circle: low expression, blue dotted circle: no change in expression. *Tspo* showed low expression only in the nondeleted exon 4 (positive control), whereas the deleted exons 2/3 are far away from the diagonal line (negative control). Scatter plots of mitochondrial cholesterol-binding protein-encoding genes in E, adrenal glands and F, lungs with 2 value differences of total base pair read counts in $\log_2$ scale. Mitochondrial cholesterol-binding proteins were retrieved from MitoCarta and a previous publication [31, 32]. Red: high expression, green, low expression. Two highlighted genes, *Apoo* and *Slc25a13*, likely play a role in compensating for TSPO depletion.

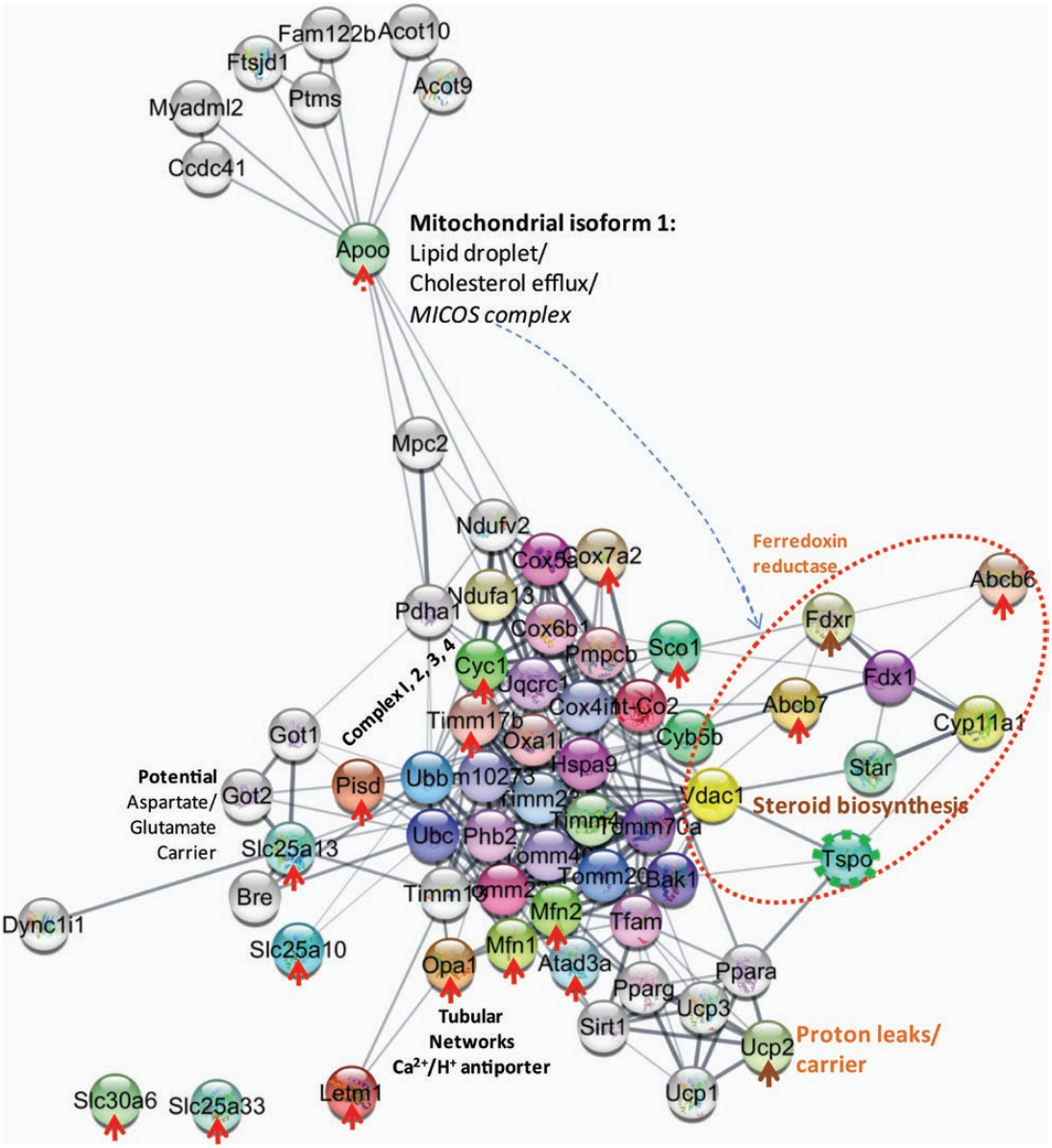

Figure 12. The compensatory mechanism after *Tspo* deletion involves upregulation of mitochondrial cholesterol-binding protein-encoding genes. The protein-protein interaction network was produced from the STRING database with medium confidence (0.400) and 20 interactions per each query proteins from the first (color) shell of interaction plus the second (white) shell of interactions and visualized using the Cytoscape plugin AllegroLayout (version 2.2.2; AllegroVivia, Inc) with the option of weak clustering visualization [52]. Red arrows: mitochondrial cholesterol-binding proteins, dark brown arrows: 2 mitochondrial proteins (UCP2 and FDXR) that have dramatic differences in base pair read counts between wild-type (*Tspo*$^{+/+}$) and homozygous (*Tspo*$^{-/-}$); Green dashed circle: position of translocator protein (TSPO) and red dotted oval: highlight of steroidogenic genes. Exon-based: *Apoo, Cox7a2, Cyb5b, Cyc1, Letm1, Mfn1, Mfn2, Ndufa13, Pisd, Sco1, Slc25a10, Slc25a13, Slc25a33, Slc30a6, Timm17b, Timm44, Abcb6, Abcb7, Atad3a,* and *Opa1*; gene-based: *Fdxr* and *Ucp2*.

there have been as many as 90 publications using the *Amhr2*-Cre–based gene knockout method [17]. The *Amhr2*-Cre/LoxP system was initially used by Morohaku et al to generate *Tspo* cKO mice [8]. In this study, the authors used cHO (*Tspo*$^{fl/fl}$-*Amhr2*$^{cre/+}$; TSPO*c*Δ/Δ, the nomenclature used by the authors vs *Amhr2*-Cre$^{+/-}$, *Tspo*$^{fl/fl}$, nomenclature used herein) mice to cross back with homozygous *Tspo*-floxed mice (*Tspo*$^{fl/fl}$) in an effort to generate

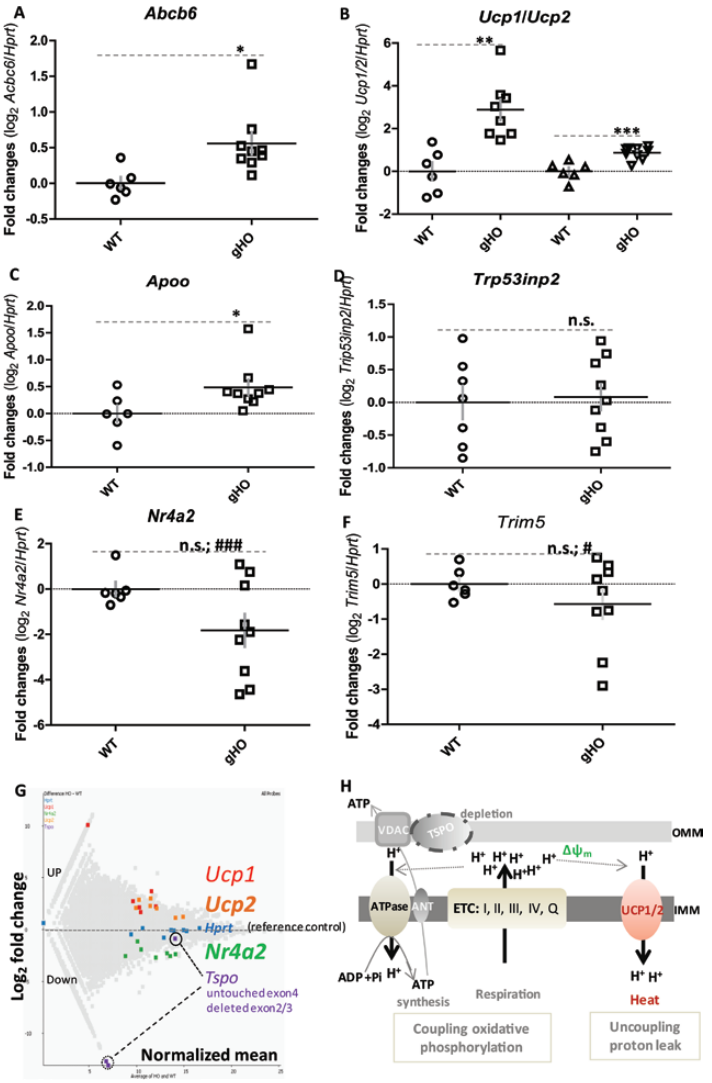

Figure 13. Validation of the RNA-sequencing (RNA-seq) analysis by real-time polymerase chain reaction (PCR). Total RNA was extracted from adrenal glands from wild-type (WT) (*Tspo*$^{+/+}$) vs homozygous (HO) (*Tspo*$^{-/-}$) mice. The expression of each gene relative to *Hprt* was determined by real-time-PCR and graphed as dot plots. Results are expressed as fold changes in $\log_2$ value, and for each sample the fold change in gene expression was calculated over its mean expression in WT samples. Data are presented as means ± SEM (indicated as cross) from 7 to 9 animals (depicted as dots/squares), each performed in triplicate. A to D, Upregulated genes, *Abcb6*, *Ucp2*, *Apoo*, and *Trp53inp2*. E and F, Downregulated genes, *Nr4a2* and *Trim5*. *P* less than .05, ***, *P* less than .001, and n.s., nonsignificant, Student t tests (n = 7-9 animals per group). #, *P* less than .01 and ###, *P* less than .001, F test to compare variances. G, Highlighted *Ucp1*, *Ucp2*, and *Nr4a2* genes within the MA plot used to visualize the differential expression analysis of the mouse adrenal RNA-seq data. *Hprt*, used as reference gene, and *Tspo*, a negative/positive control, are shown. Points indicate individual exons, x axis indicates the normalized mean, and y axis indicates the $\log_2$-fold change. Red/orange, upregulated *Ucp1* and *Ucp2*; Green, downregulated *Nr4a2*; blue, reference gene *Hprt*, and purple, negative/positive control gene *Tspo*. H, Diagram of the main upregulated *Ucp1* and *Ucp2* genes in relation to the proton leak and mitochondrial membrane potential ($\Delta\psi_m$). Protons (H^+) are extruded from the inside (mitochondrial matrix) to the outside of the, inner mitochondrial membrane (IMM), thus forming an electrochemical proton gradient, also referred to quantitatively as the $\Delta\psi_m$. Upregulated UCP1/2 induces a leak of H^+ through the IMM and "uncouples" the free energy stored in the electrochemical gradient from adenosine triphosphate (ATP) synthesis. Abbreviations: ANT, adenine nucleotide translocase; ETC, mitochondrial electron transport chain (I-IV, complex I to IV; OMM, outer mitochondrial membrane; Q, ubiquinone form of the lipophilic electron carrier [Coenzyme Q10]; UCP1/2, uncoupling protein 1/2; VDAC, voltage-dependent anion-selective channel.

cHO (TSPO*c*Δ/Δ) mice. However, we were unable to replicate the *Amhr2*-Cre–mediated testis-specific cKO mice using the same methodology [12]. Nevertheless, a common observation shared between these 2 reports is that the cKO mice produced a "WT-like" phenotype, but Morohaku et al and we came up with totally different conclusions [8, 12]. Evidence presented in these reports shows a lack of function at early embryonic stages in the presence of *Amhr2*-Cre, suggesting that one or both of the floxed alleles in TSPO*c*Δ/Δ mice used was "defective." Thus, the produced offspring are either all WT or gHE with only an 8.3% chance of being one of the cHO genotypes (*Amhr2*-Cre$^{+/-}$, *Tspo*$^{fl*/fl}$; and *Amhr2*-Cre$^{+/-}$, *Tspo*$^{fl/-}$) because of the strong genetic linkage between the *Tspo* and *Amhr2* genes. Our data suggest caution should be used when interpreting data generated using the *Amhr2*-Cre to produce cKO mice because *Amhr2*-Cre could also serve as a "global deleter" to generate gKO mice. Indeed, our findings provide an explanation of the data published using the *Amhr2*-Cre to generate an ovarian cKO for β-catenin that led to unexpected recombination in a wide range of tissues [56], as well as the partial depletion of TSPO in the mouse ovary, which actually suggests that these are gHE mice [8]. There is also another possibility that because the cells at this early embryonic developmental stage remain pluripotent, some cells that have been deleted for *Tspo* might die (if TSPO protein is required at that stage for cell survival), but they might be replaced by the pluripotent "WT" (or *Tspo* undeleted) cells leading to normal development. *Amhr2*-Cre would then be reactivated later during development allowing for tissue-specific gene ablation. This possibility is unlikely to occur but remains to be tested further.

During the characterization of the *Amhr2*-Cre–mediated *Tspo* gKO, we examined tissues other than the well-known *Amhr2*-target tissues (gonads). One interesting finding is that *Tspo* was sparsely but strongly expressed in the brain, which is in agreement with our previous report using immunofluorescence [12]. Numerous studies have shown that *Tspo* is mainly expressed in brain microglia cells [57, 58]. These observations are also agree with data using radiolabeled PK 11195 and/or other TSPO ligands in positron emission tomography to assess its expression in rodent and human brain [59-61]. However, recent reports suggested TSPO was extremely low in the brain when assessed by immunohistochemistry and immunoblot analyses [28, 62, 63]. This discrepancy raises the question of the availability of sensitive and specific antibodies for immunodetection of TSPO in the brain. In general, any negative reports should provide more experimental controls and be very cautious in their interpretation of the results, which may be due to a flawed experimental system.

Free cholesterol has been shown to be toxic to cells [64], and its detoxification has to be either through cholesterol esterification and storage into LDs or metabolism into hydrosoluble hydroxycholesterols or steroids in steroidogenic tissues. The LDs in steroidogenic tissues are mainly composed of cholesteryl esters, which differ from the LDs in adipose tissues that mainly consist of triglycerides [45, 65]. KO or knockdown of the genes involved in steroid biosynthesis results in LD accumulation, indicating lack of availability of free cholesterol for steroid formation. This is the case for *Tspo* [12, 14], *Star* [13, 66], *Cyp11a1* [67], *Cyp11b2* [68], and *Nr5a1* (SF-1) [69]. Indeed, almost all mouse tissues examined herein showed changes in neutral lipid accumulation under the TSPO deficiency, in agreement with a recent study we performed in the rat [14], and also it was positively correlated with elevated *Aug1* gene expression [70]. Even during the development of Leydig cells, the appearance or disappearance of cytoplasmic LDs is one of the visible phenotypes used to establish the developmental stage of the cell [71, 72]. Taken together with the fact that TSPO is a high-affinity cholesterol-binding protein extremely abundant in the outer mitochondrial membrane of steroidogenic cells, and the vast literature on the effects of TSPO drug ligands on steroid formation in various tissues and animal models [1, 2, 5, 73], these findings indicate that TSPO must play a regulatory role in steroid formation.

Despite the changes seen in LD accumulation, the effects seen in circulating steroid hormone levels are not as dramatic as one would expect. We noted, however, a significant 50% reduction both in intratesticular and circulating testosterone levels. Further analysis of the ability of Leydig cell preparations isolated from WT and *Tspo* gKO mice demonstrated the

lack of *Tspo* gKO Leydig cells to respond to hCG in terms of testosterone formation. This result is similar to that reported using steroidogenic cell *(Sf1)*-targeted *Tspo* cKO mice that failed to respond to ACTH stimulation [12]. In the present studies, we did not see an effect of basal circulating corticosterone levels in agreement with data reported with *Sf1*-targeted *Tspo* cKO mice, suggesting that basal, hormone-independent, steroid production by adrenal and Leydig cells is not affected by the lack of TSPO.

We were surprised by the slight but significant increase in *Tspo* gKO testis weight that we cannot explain. However, we were not surprised by the lack of changes in seminal vesicle, kidney, and epididymis weights, some of which are androgen-responsive organs. Over the years the mouse, although a great model for genetic manipulation, unlike the rat, has been proven to not be a good model to study the relationship between androgen production and testosterone effects on androgen-targeted tissues. The main difference between the mouse and rat is that the mouse testis contains very low levels of androgen binding protein (ABP), 2% to 4% of what is found in the rat [74]. Without ABP, the majority of testosterone made in the mouse testis is free and thus active. The impact of this finding was shown in studies in which the LH receptor was knocked out in mice but, nonetheless, hormone-independent testosterone formed by the Leydig cells, representing 2% of the total, was sufficient to maintain androgenicity and spermatogenesis [75]. Thus, reduction of androgen production by 50% in *Tspo* gKO mice would not affect the weight of androgen-responsive organs.

The increased presence of autophagosomes in *Tspo* gKO mouse Leydig cells, compared to WT, confirms the recently proposed hypothesis that TSPO is an element in the regulation of mitochondrial quality control in autophagy [76]. In this paper the authors elegantly showed that TSPO inhibits autophagy. Thus, in TSPO-deficient cells one should expect increased autophagy. Autophagy in normal Leydig cells has been shown to participate in testosterone production by providing cholesterol for steroidogenesis [77]. In Tspo-deficient Leydig cells, however, lack of TSPO would limit substrate availability and thus testosterone formation.

We believe that there are 2 reasons that might explain the lack of drastic changes in steroid production and mitochondrial structure, to be expected considering that TSPO comprises 2% to 4% of the outer mitochondrial membrane: first, the use of plasma membrane cholesterol, instead of LD cholesterol, for steroidogenesis as previously shown [78, 79] and second, there must be compensatory mechanisms occurring at early stages of embryo development. Previous studies showed that both TSPO and STAR are needed for the development of preimplantation embryos because lower expression of either gene leads to DNA fragmentation of preimplantation embryos, and thus apoptosis, as well as lipid accumulation [20]. In agreement with this report, the delayed development of preimplantation embryos suggests that compensation for the loss of TSPO occurs before embryo implantation. Thus, we speculate that the gHE mice used to generate gHO mice survived after preimplantation selection. This hypothesis is supported by data from another TSPO gKO mouse, the "*Guwiyang Wurra*" mouse, in which there is no linkage bias away from Mendelian ratios from crossing 2 gHE mice [58]. Additional evidence suggesting that functional adaption may occur when TSPO is absent comes from evolutionary studies showing that TSPO, a 3.5 billion year-old protein, part of the last universal common ancestor, is highly conserved across species, and a human *TSPO* deletion/mutation has not yet been reported [7, 80-82].

Genetic compensation (gene or gene network replacement) in response to gene KO, where the DNA lesion and presence of a mutated mRNA lead to relevant stress responses, is a widespread phenomenon [49, 50, 83]. Because gene deletion could elicit genetic compensatory mechanisms, gene KO may be a preferable approach to demonstrate the biological function of a gene in vivo [49]. Nevertheless, differences due to the deletion of a gene should be reflected in the transcriptome profiling. Reanalysis of previously published RNA-seq data sets indicated that the loss of TSPO invoked global gene expression changes, in contrast to a previous report [28]. Although the methodology used is state of the art, we are aware that the conclusions from RNA-seq data analysis depend not only on the sequencing coverage, depth, and numbers of reads for the transcriptome, but also on the different data analysis pipelines used in different laboratories, both of which could lead to the discrepancy. Although this is not the first RNA-seq data analysis of a TSPO-depleted tissue, it provides

information for the first time regarding transcriptome changes, validated by real-time PCR, that likely, at least in part, provides the biological basis for the compensation to the *Tspo* deletion. Such transcriptome changes involved in genetic network compensation for a lost gene can provide a reference point for properly interpreting nonvisible phenotypes after gene deletion, which could be traced back to the early stages of preimplantation embryo development, such as that shown in this report [49, 50, 83, 84].

TSPO-deletion–induced compensatory mechanisms could become activated at various steps in the process of steroid hormone formation. Despite previous evidence showing that TSPO is involved in cholesterol import into mitochondria, the rate-limiting step in steroid biosynthesis [1], the complete or partial loss of this protein may change the cell processes involved in the regulation of cholesterol storage, trafficking, and availability in a distinct way. From our analysis of mitochondrial-related gene expression profiles, several genes were identified that showed changes in their expression levels in response to TSPO deletion. Some of these genes encode cholesterol binding proteins and/or are involved in cholesterol metabolism [32, 85-89], and existing literature supports their role in steroid hormone biosynthesis. Indeed, silencing the *APOO* gene leads to overexpression of *UCP2* in HepG2 cells, and *APOO* expression has been shown to be induced by oleic acid, whereas oleic acid and/or its activated form oleoyl-CoA boosts progesterone biosynthesis in hormone-dependent steroidogenic MA-10 Leydig cells [90, 91]. UCP1 and UCP2 are both required for mitochondrial protein leakage, which is likely involved in the reduced mitochondrial membrane potential [51, 92, 93]. In addition, SLC25A13 catalyzes the calcium-dependent exchange of cytoplasmic glutamate with mitochondrial aspartate and a proton across the inner mitochondrial membrane, and its activation is strongly dependent on mitochondrial membrane potential likely via TSPO [51, 94]. Also, *Nr4a2* (or *Nurr1*), downregulated under TSPO deficiency, is involved in the regulation of adrenal aldosterone production likely via increasing the adrenal principal isoform of 3β-hydroxysteroid dehydrogenase (3β-HSD), HSD3B2 [95, 96].

In conclusion, our data provide strong evidence that the *Amhr2*-Cre mediated the generation of a *Tspo* gKO, suggesting that *Amhr2*-Cre may have wide application as a global "Cre deleter" in the mouse. Our data also show that TSPO deficiency leads to delayed preimplantation embryo development, and disturbed neutral lipid accumulation and steroid biosynthesis, as well as a compensatory gene (genetic) network in response to the TSPO genetic depletion.

Acknowledgments

We thank Dr J. Low-Marchelli (The Jackson Laboratory) for technical advice, Drs S. Vidal, A. Midzak, and D. Bernard (McGill University); Dr R. Behringer (The University of Texas MD Anderson Cancer Center); and M. Culty (University of Southern California) for insightful comments and suggestions. We thank A. Boisvert (Research Institute of the McGill University Health Centre; RI MUHC) for mouse dissection, Dr J. Li (RI MUHC) for advice on the Rosa-mT/mG mouse, and Dr A.F. Parlow (National Hormone Pituitary Program, Torrance, CA) for providing the hCG. We also thank the Immunophenotyping and Molecular Imaging Platforms of the Research Institute of the RI MUHC, N. Laughren and S. Loucao of the animal facility of the RI MUHC for help with handling laboratory animals, and A. Rodriguez (University of Southern California) for technical assistance with transmission electron microscopy.

Financial Support: This work was supported by grants from the Canadian Institutes of Health Research (MOP125983 and PJT148659), the National Institutes of Health (R01 AG21092), a Canada Research Chair in Biochemical Pharmacology, and the John Stauffer Dean's Chair in Pharmaceutical Sciences (University of Southern California).

Additional Information

Correspondence: Vassilios Papadopoulos, DPharm, PhD, Department of Pharmacology and Pharmaceutical Sciences, School of Pharmacy, University of Southern California, 1985 Zonal Avenue, 7th Floor, Los Angeles, California 90089. E-mail: vpapadop@usc.edu.

Disclosure Summary: The authors have nothing to disclose.

Data Availability: All data generated or analyzed during this study are included in this published article or in the data repositories listed in References.

References and Notes

1. Papadopoulos V, Baraldi M, Guilarte TR, et al. Translocator protein (18kDa): new nomenclature for the peripheral-type benzodiazepine receptor based on its structure and molecular function. *Trends Pharmacol Sci.* 2006;**27**(8):402–409.
2. Rupprecht R, Papadopoulos V, Rammes G, et al. Translocator protein (18 kDa) (TSPO) as a therapeutic target for neurological and psychiatric disorders. *Nat Rev Drug Discov.* 2010;**9**(12):971–988.
3. Midzak A, Rone M, Aghazadeh Y, Culty M, Papadopoulos V. Mitochondrial protein import and the genesis of steroidogenic mitochondria. *Mol Cell Endocrinol.* 2011;**336**(1-2):70–79.
4. Rone MB, Fan J, Papadopoulos V. Cholesterol transport in steroid biosynthesis: role of protein-protein interactions and implications in disease states. *Biochim Biophys Acta.* 2009;**1791**(7):646–658.
5. Papadopoulos V, Aghazadeh Y, Fan J, Campioli E, Zirkin B, Midzak A. Translocator protein-mediated pharmacology of cholesterol transport and steroidogenesis. *Mol Cell Endocrinol.* 2015;**408**:90–98.
6. Rone MB, Midzak AS, Issop L, et al. Identification of a dynamic mitochondrial protein complex driving cholesterol import, trafficking, and metabolism to steroid hormones. *Mol Endocrinol.* 2012;**26**(11):1868–1882.
7. Fan J, Papadopoulos V. Evolutionary origin of the mitochondrial cholesterol transport machinery reveals a universal mechanism of steroid hormone biosynthesis in animals. *PloS One.* 2013;**8**(10):e76701.
8. Morohaku K, Pelton SH, Daugherty DJ, Butler WR, Deng W, Selvaraj V. Translocator protein/peripheral benzodiazepine receptor is not required for steroid hormone biosynthesis. *Endocrinology.* 2014;**155**(1):89–97.
9. Tu LN, Morohaku K, Manna PR, et al. Peripheral benzodiazepine receptor/translocator protein global knock-out mice are viable with no effects on steroid hormone biosynthesis. *J Biol Chem.* 2014;**289**(40):27444–27454.
10. Tu LN, Zhao AH, Stocco DM, Selvaraj V. PK11195 effect on steroidogenesis is not mediated through the translocator protein (TSPO). *Endocrinology.* 2015;**156**(3):1033–1039.
11. Zhao AH, Tu LN, Mukai C, et al. Mitochondrial translocator protein (TSPO) function is not essential for heme biosynthesis. *J Biol Chem.* 2016;**291**(4):1591–1603.
12. Fan J, Campioli E, Midzak A, Culty M, Papadopoulos V. Conditional steroidogenic cell-targeted deletion of TSPO unveils a crucial role in viability and hormone-dependent steroid formation. *Proc Natl Acad Sci U S A.* 2015;**112**(23):7261–7266.
13. Caron KM, Soo SC, Wetsel WC, Stocco DM, Clark BJ, Parker KL. Targeted disruption of the mouse gene encoding steroidogenic acute regulatory protein provides insights into congenital lipoid adrenal hyperplasia. *Proc Natl Acad Sci U S A.* 1997;**94**(21):11540–11545.
14. Owen DR, Fan J, Campioli E, et al. TSPO mutations in rats and a human polymorphism impair the rate of steroid synthesis. *Biochem J.* 2017;**474**(23):3985–3999.
15. Li H, Yao Z, Degenhardt B, Teper G, Papadopoulos V. Cholesterol binding at the cholesterol recognition/ interaction amino acid consensus (CRAC) of the peripheral-type benzodiazepine receptor and inhibition of steroidogenesis by an HIV TAT-CRAC peptide. *Proc Natl Acad Sci U S A.* 2001;**98**(3):1267–1272.
16. Owen DR, Yeo AJ, Gunn RN, et al. An 18-kDa translocator protein (TSPO) polymorphism explains differences in binding affinity of the PET radioligand PBR28. *J Cereb Blood Flow Metab.* 2012;**32**(1):1–5.
17. Selvaraj V, Tu LN, Stocco DM. Crucial role reported for TSPO in viability and steroidogenesis is a misconception. commentary: conditional steroidogenic cell-targeted deletion of TSPO unveils a crucial role in viability and hormone-dependent steroid formation. *Front Endocrinol (Lausanne).* 2016;**7**:91.
18. *RRID:AB_10862345. PBR antibody [EPR5384].* SciCrunch website. https://scicrunch.org/resolver/AB_10862345. Accessed December 10, 2019.
19. *RRID:AB_2534016. Donkey anti-Rabbit IgG (H+L) Highly Cross-Adsorbed Secondary Antibody, Alexa Fluor 546.* SciCrunch website. https://scicrunch.org/resolver/AB_2534016. Accessed December 10, 2019.
20. Lee H, Kim J, Yang H. Steroidogenic acute regulatory protein (StAR) and peripheral-type benzodiazepine receptor (PBR) are decreased in human apoptotic embryos. *Anim Cells Syst.* 2011;**15**(3):8.

21. Mehlem A, Hagberg CE, Muhl L, Eriksson U, Falkevall A. Imaging of neutral lipids by oil red O for analyzing the metabolic status in health and disease. *Nat Protoc.* 2013;**8**(6):1149–1154.
22. Liu Y, Dettin LE, Folmer J, Zirkin BR, Papadopoulos V. Abnormal morphology of spermatozoa in cytochrome P450 17alpha-hydroxylase/17, 20-lyase (CYP17) deficient mice. *J Androl.* 2007;**28**(3):453–460.
23. Salva A, Klinefelter GR, Hardy MP. Purification of rat Leydig cells: increased yields after unit-gravity sedimentation of collagenase-dispersed interstitial cells. *J Androl.* 2001;**22**(4):665–671.
24. Payne AH, Wong KL, Vega MM. Differential effects of single and repeated administrations of gonadotropins on luteinizing hormone receptors and testosterone synthesis in two populations of Leydig cells. *J Biol Chem.* 1980;**255**(15):7118–7122.
25. Cao F, Fukuda A, Watanabe H, Kono T. The transcriptomic architecture of mouse Sertoli cell clone embryos reveals temporal–spatial-specific reprogramming. *Reproduction.* 2013;**145**(3):277–288.
26. Xie D, Chen CC, Ptaszek LM, et al. Rewirable gene regulatory networks in the preimplantation embryonic development of three mammalian species. *Genome Res.* 2010;**20**(6):804–815.
27. Xue Z, Huang K, Cai C, et al. Genetic programs in human and mouse early embryos revealed by single-cell RNA sequencing. *Nature.* 2013;**500**(7464):593–597.
28. Wang H, Zhai K, Xue Y, et al. Global deletion of TSPO does not affect the viability and gene expression profile. *PloS One.* 2016;**11**(12):e0167307.
29. Afgan E, Baker D, van den Beek M, et al. The Galaxy platform for accessible, reproducible and collaborative biomedical analyses: 2016 update. *Nucleic Acids Res.* 2016;**44**(W1):W3–W10.
30. Kent WJ, Sugnet CW, Furey TS, et al. The human genome browser at UCSC. *Genome Res.* 2002;**12**(6):996–1006.
31. Calvo SE, Clauser KR, Mootha VK. MitoCarta2.0: an updated inventory of mammalian mitochondrial proteins. *Nucleic Acids Res.* 2016;**44**(D1):D1251–D1257.
32. Hulce JJ, Cognetta AB, Niphakis MJ, Tully SE, Cravatt BF. Proteome-wide mapping of cholesterol-interacting proteins in mammalian cells. *Nat Methods.* 2013;**10**(3):259–264.
33. Fan J, Rone MB, Papadopoulos V. Translocator protein 2 is involved in cholesterol redistribution during erythropoiesis. *J Biol Chem.* 2009;**284**(44):30484–30497.
34. Letts VA, Valenzuela A, Kirley JP, Sweet HO, Davisson MT, Frankel WN. Genetic and physical maps of the stargazer locus on mouse chromosome 15. *Genomics.* 1997;**43**(1):62–68.
35. Casares P. A corrected Haldane's map function to calculate genetic distances from recombination data. *Genetica.* 2007;**129**(3):333–338.
36. Weeks DE, Tang X, Kwon AM. Casares' map function: no need for a 'corrected' Haldane's map function. *Genetica.* 2009;**135**(3):305–307.
37. Haldane JBS. The combination of linkage values, and the calculation of distance between the loci of linked factors. *J Genet.* 1919;**8**:299–309.
38. Muzumdar MD, Tasic B, Miyamichi K, Li L, Luo L. A global double-fluorescent Cre reporter mouse. *Genesis.* 2007;**45**(9):593–605.
39. Jedrusik A. Making the first decision: lessons from the mouse. *Reprod Med Biol.* 2015;**14**(4):135–150.
40. Karlstetter M, Nothdurfter C, Aslanidis A, et al. Translocator protein (18 kDa) (TSPO) is expressed in reactive retinal microglia and modulates microglial inflammation and phagocytosis. *J Neuroinflammation.* 2014;**11**:3.
41. Daugherty DJ, Chechneva O, Mayrhofer F, Deng W. The hGFAP-driven conditional TSPO knockout is protective in a mouse model of multiple sclerosis. *Sci Rep.* 2016;**6**:22556.
42. Mirzaei N, Tang SP, Ashworth S, et al. In vivo imaging of microglial activation by positron emission tomography with [(11)C]PBR28 in the 5XFAD model of Alzheimer's disease. *Glia.* 2016;**64**(6):993–1006.
43. Maeda J, Higuchi M, Inaji M, et al. Phase-dependent roles of reactive microglia and astrocytes in nervous system injury as delineated by imaging of peripheral benzodiazepine receptor. *Brain Res.* 2007;**1157**:100–111.
44. Li Q, Zhang P, Zhang C, et al. DDX3X regulates cell survival and cell cycle during mouse early embryonic development. *J Biomed Res.* 2014;**28**(4):282–291.
45. Khor VK, Ahrends R, Lin Y, et al. The proteome of cholesteryl-ester-enriched versus triacylglycerol-enriched lipid droplets. *PloS One.* 2014;**9**(8):e105047.
46. Jo Y, Hartman IZ, DeBose-Boyd RA. Ancient ubiquitous protein-1 mediates sterol-induced ubiquitination of 3-hydroxy-3-methylglutaryl CoA reductase in lipid droplet-associated endoplasmic reticulum membranes. *Mol Biol Cell.* 2013;**24**(3):169–183.
47. Zhang J, Zamani M, Thiele C, et al. AUP1 (ancient ubiquitous protein 1) is a key determinant of hepatic very-low-density lipoprotein assembly and secretion. *Arterioscler Thromb Vasc Biol.* 2017;**37**(4):633–642.

48. Fan J, Campioli E, Sottas C, Zirkin B, Papadopoulos V. Data from: Amhr2-Cre-mediated global Tspo knockout. *figshare*. 2019. https://figshare.com/s/fb09e529e6d144e9181d.
49. Rossi A, Kontarakis Z, Gerri C, et al. Genetic compensation induced by deleterious mutations but not gene knockdowns. *Nature*. 2015;**524**(7564):230–233.
50. Kim S, Titcombe RF, Zhang H, et al. Network compensation of cyclic GMP-dependent protein kinase II knockout in the hippocampus by Ca2+-permeable AMPA receptors. *Proc Natl Acad Sci U S A*. 2015;**112**(10):3122–3127.
51. Fan J, Wang K, Zirkin B, Papadopoulos V. CRISPR/Cas9–mediated *TSPO* gene mutations lead to reduced mitochondrial membrane potential and steroid formation in MA-10 mouse tumor Leydig cells. *Endocrinology*. 2018;**159**(2):1130–1146.
52. Szklarczyk D, Franceschini A, Wyder S, et al. STRING v10: protein-protein interaction networks, integrated over the tree of life. *Nucleic Acids Res*. 2015;**43**(Database issue):D447–D452.
53. Koob S, Barrera M, Anand R, Reichert AS. The non-glycosylated isoform of MIC26 is a constituent of the mammalian MICOS complex and promotes formation of crista junctions. *Biochim Biophys Acta*. 2015;**1853**(7):1551–1563.
54. Turkieh A, Caubère C, Barutaut M, et al. Apolipoprotein O is mitochondrial and promotes lipotoxicity in heart. *J Clin Invest*. 2014;**124**(5):2277–2286.
55. Jamin SP, Arango NA, Mishina Y, Hanks MC, Behringer RR. Requirement of Bmpr1a for Müllerian duct regression during male sexual development. *Nat Genet*. 2002;**32**(3):408–410.
56. Hernandez Gifford JA, Hunzicker-Dunn ME, Nilson JH. Conditional deletion of beta-catenin mediated by Amhr2cre in mice causes female infertility. *Biol Reprod*. 2009;**80**(6):1282–1292.
57. Papadopoulos V, Fan J, Zirkin B. Translocator protein (18 kDa): an update on its function in steroidogenesis. *J Neuroendocrinol*. 2018;**30**(2):1282–1292.
58. Banati RB, Middleton RJ, Chan R, et al. Positron emission tomography and functional characterization of a complete PBR/TSPO knockout. *Nat Commun*. 2014;**5**:5452.
59. Herrera-Rivero M, Heneka MT, Papadopoulos V. Translocator protein and new targets for neuroinflammation. *Clin Transl Imag*. 2015;**3**(6):391–402.
60. Abid KA, Sobowale OA, Parkes LM, et al. Assessing inflammation in acute intracerebral hemorrhage with PK11195 PET and dynamic contrast-enhanced MRI. *J Neuroimaging*. 2018;**28**(2):158–161.
61. Zimmer ER, Leuzy A, Benedet AL, Breitner J, Gauthier S, Rosa-Neto P. Tracking neuroinflammation in Alzheimer's disease: the role of positron emission tomography imaging. *J Neuroinflammation*. 2014;**11**:120.
62. Tu LN, Zhao AH, Hussein M, Stocco DM, Selvaraj V. Translocator protein (TSPO) affects mitochondrial fatty acid oxidation in steroidogenic cells. *Endocrinology*. 2016;**157**(3):1110–1121.
63. Selvaraj V, Tu LN. Current status and future perspectives: TSPO in steroid neuroendocrinology. *J Endocrinol*. 2016;**231**(1):R1–R30.
64. Tabas I. Consequences of cellular cholesterol accumulation: basic concepts and physiological implications. *J Clin Invest*. 2002;**110**(7):905–911.
65. Shen WJ, Azhar S, Kraemer FB. Lipid droplets and steroidogenic cells. *Exp Cell Res*. 2016;**340**(2):209–214.
66. Hasegawa T, Zhao L, Caron KM, et al. Developmental roles of the steroidogenic acute regulatory protein (StAR) as revealed by StAR knockout mice. *Mol Endocrinol*. 2000;**14**(9):1462–1471.
67. Hu MC, Hsu NC, El Hadj NB, et al. Steroid deficiency syndromes in mice with targeted disruption of Cyp11a1. *Mol Endocrinol*. 2002;**16**(8):1943–1950.
68. Lee G, Makhanova N, Caron K, et al. Homeostatic responses in the adrenal cortex to the absence of aldosterone in mice. *Endocrinology*. 2005;**146**(6):2650–2656.
69. Hatano M, Migita T, Ohishi T, et al. SF-1 deficiency causes lipid accumulation in Leydig cells via suppression of STAR and CYP11A1. *Endocrine*. 2016;**54**(2):484–496.
70. Lohmann D, Spandl J, Stevanovic A, Schoene M, Philippou-Massier J, Thiele C. Monoubiquitination of ancient ubiquitous protein 1 promotes lipid droplet clustering. *PloS One*. 2013;**8**(9):e72453.
71. Mendis-Handagama SM, Ariyaratne HB. Differentiation of the adult Leydig cell population in the postnatal testis. *Biol Reprod*. 2001;**65**(3):660–671.
72. Chen H, Stanley E, Jin S, Zirkin BR. Stem Leydig cells: from fetal to aged animals. *Birth Defects Res C Embryo Today*. 2010;**90**(4):272–283.
73. Papadopoulos V. On the role of the translocator protein (18-kDa) TSPO in steroid hormone biosynthesis. *Endocrinology*. 2014;**155**(1):15–20.
74. Joseph DR. Structure, function, and regulation of androgen-binding protein/sex hormone-binding globulin. *Vitam Horm*. 1994;**49**:197–280.

75. Zhang FP, Pakarainen T, Poutanen M, Toppari J, Huhtaniemi I. The low gonadotropin-independent constitutive production of testicular testosterone is sufficient to maintain spermatogenesis. *Proc Natl Acad Sci U S A*. 2003;**100**(23):13692–13697.
76. Gatliff J, East D, Crosby J, et al. TSPO interacts with VDAC1 and triggers a ROS-mediated inhibition of mitochondrial quality control. *Autophagy*. 2014;**10**(12):2279–2296.
77. Zhu Y, Yin Q, Wei D, Yang Z, Du Y, Ma Y. Autophagy in male reproduction. *Syst Biol Reprod Med*. 2019;**65**(4):265–272.
78. Freeman DA. Regulation of the cholesterol ester cycle of cultured Leydig tumor cells. *Eur J Biochem*. 1987;**164**(2):351–356.
79. Venugopal S, Martinez-Arguelles DB, Chebbi S, Hullin-Matsuda F, Kobayashi T, Papadopoulos V. Plasma membrane origin of the steroidogenic pool of cholesterol used in hormone-induced acute steroid formation in leydig cells. *J Biol Chem*. 2016;**291**(50):26109–26125.
80. Fan J, Lindemann P, Feuilloley MG, Papadopoulos V. Structural and functional evolution of the translocator protein (18 kDa). *Curr Mol Med*. 2012;**12**(4):369–386.
81. Batoko H, Veljanovski V, Jurkiewicz P. Enigmatic translocator protein (TSPO) and cellular stress regulation. *Trends Biochem Sci*. 2015;**40**(9):497–503.
82. Li F, Liu J, Zheng Y, Garavito RM, Ferguson-Miller S. Protein structure. Crystal structures of translocator protein (TSPO) and mutant mimic of a human polymorphism. *Science*. 2015;**347**(6221):555–558.
83. El-Brolosy MA, Stainier DYR. Genetic compensation: a phenomenon in search of mechanisms. *PloS Genet*. 2017;**13**(7):e1006780.
84. Barbaric I, Miller G, Dear TN. Appearances can be deceiving: phenotypes of knockout mice. *Brief Funct Genomic Proteomic*. 2007;**6**(2):91–103.
85. Lamant M, Smih F, Harmancey R, et al. ApoO, a novel apolipoprotein, is an original glycoprotein up-regulated by diabetes in human heart. *J Biol Chem*. 2006;**281**(47):36289–36302.
86. Song YZ, Li BX, Chen FP, et al. Neonatal intrahepatic cholestasis caused by citrin deficiency: clinical and laboratory investigation of 13 subjects in mainland of China. *Dig Liver Dis*. 2009;**41**(9):683–689.
87. Blanc J, Alves-Guerra MC, Esposito B, et al. Protective role of uncoupling protein 2 in atherosclerosis. *Circulation*. 2003;**107**(3):388–390.
88. Wasilewski M, Semenzato M, Rafelski SM, Robbins J, Bakardjiev AI, Scorrano L. Optic atrophy 1-dependent mitochondrial remodeling controls steroidogenesis in trophoblasts. *Curr Biol*. 2012;**22**(13):1228–1234.
89. Issop L, Fan J, Lee S, et al. Mitochondria-associated membrane formation in hormone-stimulated Leydig cell steroidogenesis: role of ATAD3. *Endocrinology*. 2015;**156**(1):334–345.
90. Wu CL, Zhao SP, Yu BL. Microarray analysis provides new insights into the function of apolipoprotein O in HepG2 cell line. *Lipids Health Dis*. 2013;**12**:186.
91. Castillo AF, Cornejo Maciel F, Castilla R, et al. cAMP increases mitochondrial cholesterol transport through the induction of arachidonic acid release inside this organelle in Leydig cells. *Febs J*. 2006;**273**(22):5011–5021.
92. Azzu V, Jastroch M, Divakaruni AS, Brand MD. The regulation and turnover of mitochondrial uncoupling proteins. *Biochim Biophys Acta*. 2010;**1797**(6-7):785–791.
93. Krauss S, Zhang CY, Lowell BB. A significant portion of mitochondrial proton leak in intact thymocytes depends on expression of UCP2. *Proc Natl Acad Sci U S A*. 2002;**99**(1):118–122.
94. Satrústegui J, Pardo B, Del Arco A. Mitochondrial transporters as novel targets for intracellular calcium signaling. *Physiol Rev*. 2007;**87**(1):29–67.
95. Bassett MH, Suzuki T, Sasano H, White PC, Rainey WE. The orphan nuclear receptors NURR1 and NGFIB regulate adrenal aldosterone production. *Mol Endocrinol*. 2004;**18**(2):279–290.
96. Ota T, Doi M, Yamazaki F, et al. Angiotensin II triggers expression of the adrenal gland zona glomerulosa-specific 3β-hydroxysteroid dehydrogenase isoenzyme through de novo protein synthesis of the orphan nuclear receptors NGFIB and NURR1. *Mol Cell Biol*. 2014;**34**(20):3880–3894.